

NASA CONTRACTOR REPORT



NASA CR-54421

NASA CR-54421

VAPOR-FILLED THERMIONIC CONVERTERS

**PREPARED BY K. G. HERNQVIST (Project Scientist),
J. R. FENDLEY, JR. AND J. D. LEVINE**

APPROVED BY P. RAPPAPORT, Project Supervisor

FINAL REPORT

Prepared under Contract No. NAS 3-4173



**RADIO CORPORATION OF AMERICA
RCA LABORATORIES
PRINCETON, NEW JERSEY**

for

**NATIONAL AERONAUTICS & SPACE ADMINISTRATION • WASHINGTON, D. C. • APRIL 1965
LEWIS RESEARCH CENTER**

FOREWORD

This report includes theoretical and experimental results from studies of cesium surface adsorption and cesium plasma phenomena. A comprehensive Mid-Point Report (NASA CR-54194) covering work done under this contract was issued in September 1964. The most significant parts of that report have been published in the *Proceedings of the Thermionic Conversion Specialist Conference*, Cleveland, Ohio, October 1964. Only summaries of that work are included in this Final Report.

We wish to acknowledge the encouragement and support of Mr. Harold Nastelin and Mr. Herman Schwartz of the NASA Lewis Research Center.

ABSTRACT

26628

Theoretical studies necessary for interpreting experimental conductivity data of cesium on insulators have been completed. Starting from the Schrödinger equation for a single adsorbed cesium atom, wave functions and their properties have been compiled. This information and Kopineck's integrals are used to compute the tunneling (resonance) energy between two adsorbed cesium atoms which is then generalized to an entire array of adsorbed cesium atoms. One of the most important consequences of the theory is that, to a first approximation, conductivity should be proportional to the cesium pressure squared. The experimental data verify this and also verify other anticipated dependences on dielectric constant and surface contamination. The cesium adsorption heat on clean alumina and Pyrex surfaces is calculated to be 0.85 eV; and the large configurational entropy term, $\Delta S/k \sim 6$, seems to indicate a long-range order in agreement with certain low-energy electron diffraction (LEED) studies. Data obtained under contaminated conditions have shown that adsorbed hydrogen causes the conductivity to increase following a $2/3$ -power law, while leaving the cesium adsorption heat invariant.

Various measurements of arc drop and anode work function are reported. Arc drop is found to be nearly 0.5 volt for cathode temperature in the range 1300 to 1500°K and current density of 6 to 12 A/cm². Anode work function with a high cesium coverage has been found to be equal to or greater than 1.93 V.

A method is described for measuring the work function of metal surfaces coated with adsorbed cesium or with a combination of cesium and oxygen.

An analysis of the effects of reverse currents in thermionic converters is presented. It is shown that reverse currents cause a contribution to the arc drop and also impose limiting conditions on the useful range of anode work functions.

Author

TABLE OF CONTENTS

<i>Section</i>	<i>Page</i>
FOREWORD	ii
ABSTRACT	iii
LIST OF ILLUSTRATIONS	vi
INTRODUCTION	1
I. ADSORPTION OF CESIUM ON INSULATORS	7
A. Introduction to Cesium Adsorption on Insulators	2
B. Nodal Hydrogenic Wave Functions	3
1. Potential Function	4
2. Wave Functions	5
3. Expectation Values	8
4. Discussion	8
C. Gradual Distortion of Hydrogenic Wave Functions	9
1. Surface Hamiltonian and Wave Function	9
2. Variational Calculation	11
3. Application to a Coulombic Hamiltonian	14
4. Application to Cesium on Insulators	17
D. Theory of Tunneling Conductivity	18
1. Tunneling Equation	18
2. Tunneling Energy	20
3. Phonon Energy	23
4. Parametric Analysis	25
E. Equation of State	27
F. Electrical Conductivity Caused by Adsorbed Cesium on Insulator Surfaces	30
G. Comparison of Theory with Experiment	30
H. Conclusions Drawn from Cesium Adsorption on Insulators	34
II. WORK FUNCTION STUDIES	36
A. Cesium Reference Anodes	36
B. A Cesium Beam Method for Work Function Measurement	36
1. Introduction	36
2. Details of the Beam Method	36
3. Experimental Results	37
III. REVERSE CURRENTS IN THERMIONIC CONVERTERS	38
CONCLUSIONS AND RECOMMENDATIONS	39
REFERENCES	40

LIST OF ILLUSTRATIONS

Figure		Page
1	Potential of an electron as a function of position. A dielectric crystal occupies the half space $z \geq 0$ and a positive donor ion is located at the surface $z = 0$. In the approximation discussed in the text, the solid line is the effective potential ..	5
2	Schematic angular orbitals for some surface donor wave functions	7
3	Idealized potential function of a hydrogenic atom located in the surface plane $z = 0$. W represents a step function which is constant for negative z	10
4	Dimensionless energy ϵ and dipole moment M_d plotted versus dimensionless wall potential ω . As ω increases to infinity, ϵ and M_d both increase and approach unity	13
5	Fractional bond character variation with wall potential. c_2^2 = covalent fraction, c_1^2 = ionic fraction, $2c_1c_2\Delta$ = resonance fraction	14
6	Variation of Coulombic energy levels as the wall potential is turned on. Degeneracy of constant n shells is greatly exaggerated to show splitting into bonding states on the right side of the figure and antibinding states are shown as arrows pointing to the crystal continuum	15
7	Variation of three wave functions as the wall potential is turned on. Wall squeezes wave functions into the dielectric with no new radial nodes arising	17
8	Conduction due to a line of donor atoms on a surface. (a) Wave functions. (b) Energy states as a function of position. Wavy lines indicate phonon transitions which dissipate electrical energy	18
9	Dimensionless tunneling energy versus a^{-2} , which is proportional to coverage. The dashed line is an adequate approximation for a large range of E_t/E_i	22
10	Pyramidal molecule consisting of one cesium ion nestled on top of three oxygen ions. Phonons are transferred via the vertical molecular vibrations	24
11	Parametric theoretical plot of tunneling conductivity versus coverage for various values of dielectric constant. Shaded area indicates region where data have been obtained	26
12	Master plot of constant conductivity versus reciprocal bath and surface temperatures, taken under "clean" conditions. Data refer to Diamonite ceramic, Frenchtown ceramic, and sapphire. Lines follow semiempirical Arrhenius formula	31
13	Master plot of Blackford's cesium on Pyrex glass data. The semiempirical line formula is similar to that of cesium on ceramic under "clean" conditions	32
14	Master plot of constant conductivity versus reciprocal bath and surface temperatures, taken under "unclean" conditions	32
15	Beam apparatus for work function measurement	37

INTRODUCTION

The most useful and well-established form of thermionic converter is the cesium vapor diode operated in the arc mode. Here cesium is used both in establishing desirable electrode surface properties and for space charge neutralization. It was the objective of the work done under this contract to improve the fundamental understanding of both of these functions and thus make it possible to more accurately define device limitations and to establish promising new directions for device improvements.

In the area of surface studies, the stated objective was to understand the properties of cesium adsorbed on insulator surfaces. An understanding of this basic system has been completed and is expected to be helpful in devising new electrode surface conditioning methods of interest for thermionic converters.

The plasma studies described in this report had as objective the establishment of factors affecting the arc drop. These studies have resulted in an accurate determination of the arc drop and a correlation with theory.

I. ADSORPTION OF CESIUM ON INSULATORS

by

Jules D. Levine

A. INTRODUCTION TO CESIUM ADSORPTION ON INSULATORS

Emitter and collector surfaces in thermionic energy converters are complex because of adsorbed cesium, adsorbed additive gases, and adsorbed residual gases. At present, there exists no experimental or theoretical study capable of fully interpreting these complexities. The frequently reported experimental studies of work function changes with various cesium and additive pressures do not reveal the lateral interatomic forces between the cesium and the additive gas. Present theoretical analyses of interadsorbate reactions are not based on solutions of Schrödinger's equation, and criteria for obtaining very low work function surfaces are imperfectly understood.

For one class of adsorption systems, however, there does exist a large quantity of easily interpreted experimental data and a firm theoretical foundation formulated in quantum mechanical terms. This class consists of adsorbed cesium plus an additive on an insulator substrate. It is possible in this unique system to proceed logically from (a) the one-electron Schrödinger equation, to (b) the two-body interaction, to (c) the conductivity relations, dipole moments, and equations of state. Effects of the additive gas can be analyzed. Comparisons of theory with experiment are excellent.

As stated in the Contract Objective, the purpose of the report to follow is to fully understand this unique system of cesium adsorption on insulators.

Experimental studies¹⁻³ have previously shown that there is a little chemical reaction between cesium and insulators, the data are reproducible, and a great variety of properties can be measured, such as electrical conductivity, thermoelectric effect, diffusion and kinetics of adsorption. Finally, because the insulator substrate is electrically inert, electrical effects caused by adsorbed cesium can easily be distinguished from the bulk substrate and observed over many orders in magnitude.

Theoretical studies to be described here represent an attempt to unify much of this experimental data into one coherent fabric. The approach is fundamental in the sense that there is a logical development from the general quantum theory of surface donors to the equations for electrical conductivity.

To be specific, in Section I-B the nodal wave functions of isolated donor atoms are explicitly derived, and in Section I-C the details of donor wave function distortions are calculated by a variational technique for an arbitrary surface asymmetry potential. Only fundamental constants - Planck's constant, electron mass, electronic charge, and dielectric constant - enter into the relationships. The ground state of a surface donor, like cesium on an insulator, consists of one lobe of a 2p wave function penetrating into the insulator. The formalism is simple and elegant.

In Section I-D the interactions between surface donors are considered. Explicit calculations of the quantum mechanical resonance integral between two surface donors are made, which lead to a theoretical expression for electrical conductivity. The conductivity mechanism consists of electron tunneling with phonon losses due to vibrational coupling of the donor to the lattice.

The donor phonon energy is explicitly calculated. Calculations show that conductivity should be proportional, in the first approximation, to the cesium coverage squared.

In Section I-E, the equation of state is computed which relates coverage to surface temperature and vapor bath temperature. At the low coverages of interest, the coverage is theoretically proportional to the cesium vapor pressure; also, the conductivity should theoretically be proportional to the vapor pressure squared. Two unknowns appear in the equation of state: the adsorption heat and the configurational entropy change.

Section I-F is a summary of the experimental data obtained and Section I-G is a comparison of these data with theory. Conductivity is found to be proportional to vapor pressure squared in exact agreement with theory. The adsorption heat and entropy change are unambiguously computed from the data. Theoretical dependences on dielectric constant and contaminant gases indicate long-range ordering of cesium donors. Finally, Section I-H reviews the main conclusions of this effort.

The theoretical understanding of cesium adsorption processes on insulators has gradually evolved from more primitive concepts which were discarded as more experimental and theoretical evidence was accumulated. One early conception of surface conduction through the substrate conduction band had to be discarded because, experimentally, the conduction magnitudes on glass and sapphire substrates were similar even though glass exhibits a poorly defined band structure. Another conception of adsorbed cesium diatomic molecules had to be discarded because, theoretically, cesium atom interactions yield a pressure squared dependence on conductivity and, experimentally, transient desorption experiments indicate adsorbed cesium atoms. Finally, a third conception of impurity band conduction due to cesium-cesium surface band formation had to be discarded because theoretical calculations showed that the interactions are too weak to form such a band.

The present concept of tunneling conductivity between adsorbed cesium atoms not only has a good theoretical foundation but also agrees well with experimental data taken up to the present time.

The novel and successful theoretical tools developed here could be extended next to the more complex system of cesium plus additive adsorbed on a metallic surface. The extra complexity largely arises because Wannier functions, which are stationary wave packets in metallic band theory, must be used. Such a fundamental study follows naturally from the present effort and would be especially important, considering the current trend of introducing additives into thermionic energy converters.

B. NODAL HYDROGENIC WAVE FUNCTIONS

A donor atom located on a semiconductor surface will have properties considerably different from a donor atom located in the semiconductor bulk. Three examples of surface donors would be: a phosphorus atom located on a silicon surface, a sodium atom on a sodium chloride surface, and a cesium atom on a sapphire surface. An understanding of surface donor properties is important to adsorption physics, to catalysis, to thin-film formation, and to certain electronic devices dominated by surface effects. Also, the quantum mechanical properties associated with the chosen donor potential are simple and elegant.

A surface donor atom is considered to be an ion core plus a valence electron moving about it in an atomic orbital, in accordance with quantum mechanics. Such a condition will prevail at

low temperatures and is the condition of interest. At high temperatures the donor may become ionized whereby the valence electron moves in the crystal conduction band, and Poisson's equation and Fermi-Dirac statistics must be used. We consider only the electronic structure of an isolated surface donor atom before ionization.

Many workers⁴⁻⁶ have attempted to calculate surface wave functions and energy levels by considering the adsorbate and substrate as a giant macromolecule. Because the periodicity of the crystal lattice is disturbed at the surface by the adsorbed species, new (Tamm-like) adsorption states appear, which can be calculated from quantum mechanics. The calculations are extremely complicated so that physical insight is frequently lost in the mathematics. In addition, grossly simplifying assumptions must be invoked so that energy calculations are at most qualitative.

Weisz⁷ has attempted to calculate the donor ionization energy E_i by using simple adsorption ideas. He considers E_i to be fixed by the difference of the ionization potential I of the free vapor atom and the work function ϕ_e of the crystal. According to this idea, if $I > \phi_e$ then a metallic adsorbate would not be spontaneously ionized to form a conduction electron. But a phosphorus atom ($I = 10.9$ eV) located inside a germanium crystal ($\phi_e = 4.5$ eV) is experimentally known to be easily ionized ($E_i = 0.01$ eV) even though $I > \phi_e$. Thus the $(I - \phi_e)$ criteria and the "boundary layer theory of adsorption" on which it is based⁸ are open to serious question.

The approach taken in the discussion to follow is different from the two approaches mentioned above. Essentially, it is an extension of the established quantum mechanical theory of a donor atom located within a semiconductor.⁹⁻¹¹ In this theory, the semiconductor is assumed electrically inert except for providing a dielectric constant κ . Such an assumption allows calculation of hydrogenic wave functions and energy levels which agree with experiment. For example, a simple theoretical calculation of E_i for silicon based on $\kappa = 12.0$ and effective electron mass equal to the free electron mass yields $E_i = (\text{hydrogen ionization energy})/\kappa^2$ or 0.094 eV. For comparison, E_i for Li, P, As, and Sb donors in silicon is experimentally found to be $0.041 \text{ eV} \pm 15\%$. A more realistic theoretical calculation,⁷ taking into account the separately measured effective mass tensor, yields 0.029 eV. Reasons for the discrepancy of 0.012 eV between this refined value and experiment are attributed to the effect of the donor ion core. Similar considerations hold for donors in germanium. This theory has also predicted wave functions, excited state energies, and the effect of strains, electric and magnetic fields in good agreement with experiment. Methods of extending these ideas to a donor located at the surface of a semiconductor crystal are described below. A similar analysis also applies to surface acceptors.

1. Potential Function

Consider a donor atom located on the surface of a dielectric crystal. The potential function $V(r, \theta, \phi)$ is chosen to be

$$V(r, \theta, \phi) = -e^2/\kappa r \text{ inside the dielectric} \quad (1a)$$

$$V(r, \theta, \phi) = +\infty \text{ outside the dielectric} \quad (1b)$$

which is shown by the solid line in Fig. 1. Here e is the unit electronic charge and κ is the crystal dielectric constant, taken for simplicity to be uniform up to the crystal boundary. The coordinates r , θ , and ϕ are the usual spherical coordinates arranged so that the z -axis ($z = r \cos \theta$) points in the direction perpendicular to the surface. In particular, the dielectric half-space is represented by $z > 0$, or $0 < \theta < \pi/2$, and the vacuum half-space is represented by $z < 0$, or $\pi/2 < \theta < \pi$. The potential is arbitrarily referred to zero when the valence electron is in the crystal bulk conduction band ($r \rightarrow \infty$, $\theta < \pi/2$).

The chosen potential is in fact an excellent approximation to that of a real surface donor. Qualitatively speaking, the valence electron is energetically most stable within the dielectric half-space because of the high electron affinity χ there. Quantitative statements can be made by referring to a more accurate outside potential, $\chi = e^2/r$, shown in Fig. 1 by the dashed line. The proposed infinite magnitude of V in Eq. (1b) seems justified since χ (≈ 1 eV) is frequently 10-100 times the surface donor ionization energy E_i as will be shown later. The proposed step potential of V at the surface $z = 0$ (or $\theta = \pi/2$) requires more justification. Consider points A and B in Fig. 1.

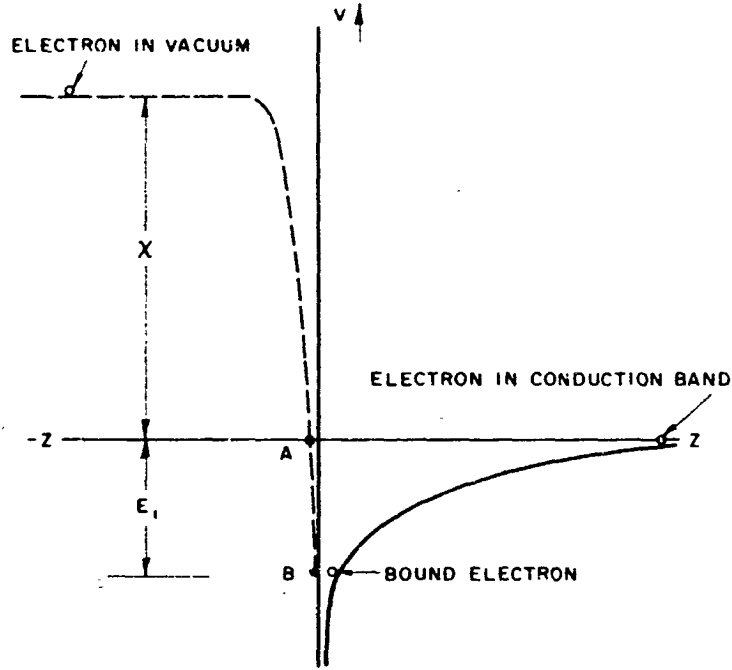


Fig. 1. Potential of an electron as a function of position. A dielectric crystal occupies the half space $z \geq 0$ and a positive donor ion is located at the surface $z = 0$. In the approximation discussed in the text, the solid line is the effective potential.

Point A is located at the conduction band level where $V = 0$ and $z_A = e^2/\chi$. Point B is located at the lowest donor level $V = -E_i$ and $z_B = e^2/(\chi + E_i)$. The difference between z_A and z_B is calculated to be $\delta = e^2 E_i / \chi^2$. Typically, for $E_i \approx 0.1$ eV and $\chi = 1$ eV, one obtains $\delta \approx 0.1 \times 13.6 / 1 \times 1 \approx 1$ Å, which is less than one lattice constant. In summary, when the potential function varies from $V = -E_i$ to $V = 0$, the potential barrier at the left of Fig. 1 varies by approximately 1 Å while the barrier at the right varies from approximately 10 Å to ∞ . Thus, the step change in the potential function at the surface seems justified for calculating surface donor energies, especially if $E_i/\chi < 0.1$.

2. Wave Functions

The Schrödinger equation for the wave function $\psi(r, \theta, \phi)$ and the donor energy E of a single valence electron is

$$\frac{\hbar^2 \nabla^2}{8\pi^2 \mu^*} \psi(r, \theta, \phi) + [E - V(r, \theta, \phi)] \psi(r, \theta, \phi) = 0 \quad (2)$$

where \hbar is Planck's constant and μ^* is the effective electron mass in the nontensor approximation.

The allowed wave functions satisfying Eqs. (1) and (2) are simply those hydrogenic wave functions which have a planar node at the crystal boundary, $\theta = \pi/2$. To be specific, the wave functions are listed below with Pauling's normalization¹²:

Outside the dielectric

$$\psi(r, \theta, \phi) = 0 \quad (3)$$

Inside the dielectric

$$\psi_{n\ell m}(r, \theta, \phi) = R_{n\ell}(r) \Theta_{\ell m}(\theta) \Phi_m(\phi) \quad (4)$$

$$R_{n\ell}(r) = - \left\{ \left(\frac{2}{\kappa n a_o^*} \right)^3 \frac{(n-\ell-1)!}{2n[(n+\ell)!]^3} \right\}^{1/2} e^{-\rho/2} \rho^\ell L_{n-\ell-1}^{2\ell+1}(\rho) \quad (5)$$

$$\Theta_{\ell m}(\theta) = \sqrt{2} \left[\frac{(2\ell-1)(\ell-|m|)!}{2(\ell+|m|)!} \right]^{1/2} P_\ell^{|m|}(\cos \theta) \quad (6)$$

$$\Phi_m(\phi) = \frac{1}{\sqrt{2\pi}} e^{im\phi} \quad (7)$$

where ρ and a_o^* are defined as

$$\rho = \frac{2r}{\kappa n a_o^*} \quad \text{and} \quad a_o^* = \frac{h^2}{4\pi^2 \mu^* e^2} \quad (8)$$

and the functions $L_{n+\ell}^{2\ell+1}(\rho)$ and $P_\ell^{|m|}(\cos \theta)$ are the associated Laguerre polynomials and the associated Legendre polynomials, respectively. From the known properties of $P_\ell^{|m|}(\cos \theta)$ it follows that the requirement of a planar node at $\theta = \pi/2$ is exactly equivalent to a "surface selection rule":

$$(\ell + m) = \text{odd} \quad (9)$$

Provided this rule is obeyed, the total wave function, equal to the sum of Eqs. (3) and (4), is continuous at the boundary, $\theta = \pi/2$, and is identically zero there. A continuity in the slopes of Eqs. (3) and (4) at the boundary is not required because of the infinite potential wall.¹³

Six consequences of the restriction to half-space and the surface selection rule, $l + m$ odd, are described below:

(1) All spherically symmetric s wave functions are forbidden for surface donors. In addition, the entire electronic shell with $n = 1$ is forbidden.

(2) The ground state of a surface donor is formed from one lobe of a 2p wave function. Schematic plots of all the allowed p, d, and f wave function orbitals for surface donors are depicted in Fig. 2. These plots represent stationary wave functions obtained from linear combinations of Eq. (4) using $l + m$ values. All of the wave functions give rise to nonzero dipole moments.

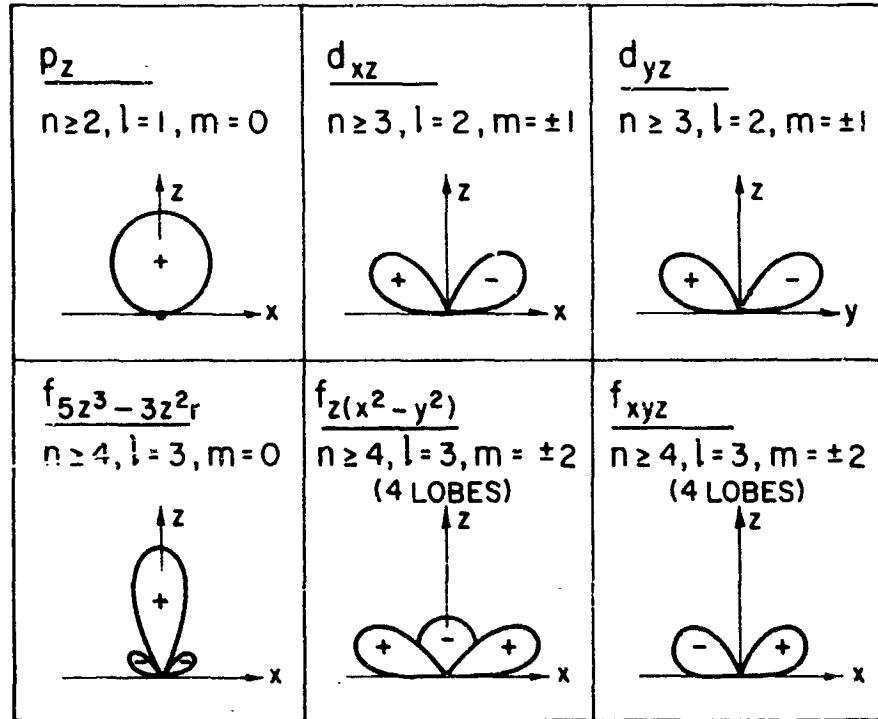


Fig. 2. Schematic angular orbitals for some surface donor wave functions.

(3) The degeneracy of a subshell of constant l is equal to $2l$, which is smaller than the value $(2l + 1)$ required in the rule's absence.

(4) The totality of electronic states with spin-up and spin-down in a complete shell of constant n is $n(n-1)$, which is about half the value $2n^2$ required in the rule's absence.

(5) Radiative dipole transitions between excited donor states are allowed, subject to the restriction $\Delta l = \pm 1$, corresponding to light polarized in the surface plane. Transitions for $\Delta l = \pm 1, m = 0$, corresponding to light polarized perpendicular to the surface plane, are forbidden.

(6) Since $\Theta_{lm}(\theta)$ of Eq. (6) vanishes by definition in the vacuum half-plane, its normalized amplitude must be multiplied by $\sqrt{2}$ in the dielectric half-plane. The required normalization factor $\sqrt{2}$ is explicitly included as the first factor of Eq. (6).

3. Expectation Values

Using the wave functions of Eqs. (4) to (9) the expectation values of any parameter W can be calculated from the definition $\bar{W} = \iiint \psi^* W \psi d\tau$. Expectation values of many parameters – electrostatic energy, potential energy, total energy, radius, orbital angular momentum, and the z component of angular momentum – are independent of the surface selection rule ($l + m$) – odd. Hence, these parameters have a direct correspondence with excited states of a donor atom immersed in the bulk of a dielectric crystal.

In particular, the energy levels E_n are given by

$$E_n = -\frac{e^2}{2\kappa^2 n^2 a_0^*} = \frac{E_H \mu^*}{\kappa^2 n^2 \mu} \quad (10)$$

where E_H is the well-known hydrogenic 1s ionization energy, 13.6 eV, and μ^*/μ is the ratio of effective to free electron mass. But because $n \geq 2$ for a surface donor, the 2p ground state energy of a surface donor corresponds to a 2p first excited state of a bulk donor. The ionization energy E_i of a surface donor is therefore 1/4 that of a bulk donor. Typically for $\kappa = 5$ and $\mu^*/\mu = 1$, the ionization energy is ≈ 0.1 eV as anticipated in Section I-B-2.

The mean radius \bar{r} is given by

$$\bar{r}_{n\ell} = n^2 \kappa a_0^* \left\{ 1 + \frac{1}{2} \left[1 - \frac{\ell(\ell+1)}{n^2} \right] \right\} \quad (11)$$

which becomes $r_{21} = 5\kappa a_0^*$ for the surface donor ground state. Typically, for $\kappa = 5$ and $\mu^*/\mu = 1$, $r_{21} = 13$ Å. *The large radius, coupled with the fact that the wave function vanishes at the center of the donor ion core, shows that the energy levels are insensitive to a local non-Coulombic potential caused by the ion core.* Hence, for nodal wave functions on a high κ crystal, the Coulombic potential function of Section I-B-2 seems to be an adequate approximation.

The mean dipole moment M is nonzero for all surface donor states due to the surface asymmetry. Its magnitude for the 2p ground state is

$$M_{2p} = \overline{ez}_{2p} = (15/4) e\kappa a_0^* \quad (12)$$

which for $\kappa = 5$ and $\mu^*/\mu = 1$ gives $M_{2p} = 43$ Debyes; this is an order of magnitude greater than dipole moments of diatomic molecules.

4. Discussion

The properties of a hydrogenlike atom placed in an electric field, a magnetic field, and a crystalline field have been thoroughly investigated in the literature, and are here extended to a different *surface field* having the potential of Eq. (1). Because only certain surface donor wave functions are allowed, the consequences of a surface effect are predicted to be much more extreme than the Stark or Zeeman effects which may be handled by ordinary perturbation theory. Whether or not the family of surface wave functions predicted here is realistic is a question to be decided by careful experimental measurements. At present, these have not been carried out for

the system of an isolated donor atom located on a semiconductor or an insulator crystal surface. Infrared spectroscopy would probably be the most informative experimental tool for this investigation.

It is a simple matter to extend the theory presented here to related problems. An extension to acceptor atoms located on semiconductor surfaces shows that similar surface energy levels are obtained, being occupied by a valence band hole instead of an electron. An extension to diatomic molecules located on semiconductor surfaces shows that axially symmetric Σ -bonds are forbidden, while π -bonds and Λ -bonds which have the acceptable planar node passing through the two nuclei are allowed. An extension to a donor atom with two or more valence electrons is more complicated but would follow the general procedure used for free atoms in the vapor state. Effects due to donor-donor interactions can also be considered, if desired. The primary interaction is a dipole-dipole repulsion which tends to keep the adsorbate atoms equidistant. Large changes in a single atom's energy levels, due to the dipole field of neighboring atoms, are unlikely.

The large dipole moments of surface donors predicted by the theory may be used in device applications for forming low work function surfaces or for extracting tunnel currents through a thin insulator.

Finally, the predictions presented here can be derived in a different way by choosing the z -axis to lie in the surface plane* and investigating the nodes of the $\Phi(\phi)$ function of Eq. (7). This approach allows one to determine, by inspection, that the degeneracy of an ℓ -subshell is ℓ -fold.

C. GRADUAL DISTORTION OF HYDROGENIC WAVE FUNCTIONS

The purpose of this section is to extend the ideas of the last section to a more general problem: the calculation of hydrogenic surface wave functions for arbitrary surface asymmetry and arbitrary atomic potential function. Such a general treatment allows one to visualize a situation where surface wave function distortions can be followed as smooth functions of surface asymmetry potential.

Consequences of these distortions are surface tension, surface dipole moment, surface free energy, and catalytic activity. For the cesium on insulator case of particular interest, this section displays the wave function distortions of a cesium atom ground state and all the excited states as a dielectric surface is approached. More important than the numerical calculations of this section, however, are the broad qualitative insights into surface phenomena.

1. Surface Hamiltonian and Wave Function

Consider an isolated positive ion located at the surface of a nonmetallic solid or liquid. The ion attracts a valence electron in a closed hydrogen-like orbit to form a surface atom. A metallic solid does not have closed valence orbitals and must be treated differently using Wannier functions.

Energy levels E of closed orbitals on nonmetallic solids can be computed from the one-electron Schrödinger equation:

$$H\psi = E\psi \quad (13)$$

*W. B. Teutsch, RCA Laboratories, personal communication.

The Hamiltonian H pertaining to the surface is idealized for simplicity to be:

$$H = H_0 + W^- \quad (14)$$

where H_0 is a spherically symmetric part and W^- is an asymmetric part due to a "surface wall," idealized as a step function:

$$W^- = \begin{cases} 0 & \text{for } z > 0 \\ W & \text{for } z < 0 \end{cases} \quad (15)$$

The coordinate z is chosen normal to the surface such that the half-plane $z > 0$ is inside the material where the wall W^- vanishes. The other half-plane $z < 0$ lies outside the material where the wall is nonzero and constant. The wall repulsive potential will be allowed to vary over the entire range $0 < W < \infty$. A sketch of the potential function V associated with H is given in Fig. 3.

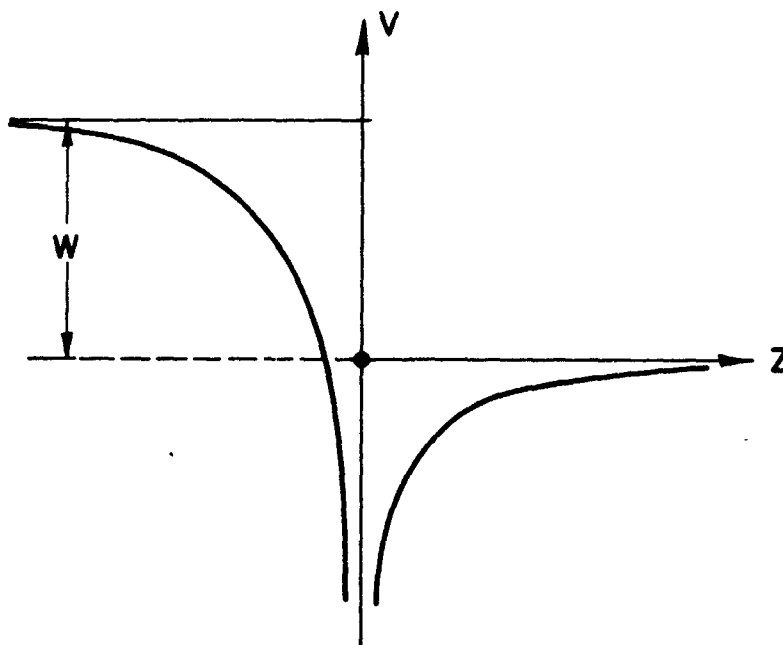


Fig. 3. Idealized potential function of a hydrogenic atom located in the surface plane $z = 0$. W represents a step function which is constant for negative z .

The wave function ψ pertaining to the surface atom bonding orbital is chosen to be the sum of a symmetric and an asymmetric part:

$$\psi = c_1 \psi_1 + c_2 \psi_2^+ \quad (16)$$

Here ψ_1 is a spherically symmetric wave function (such as a 1s hydrogenic function) satisfying the eigenvalue equation for $W = 0$

$$H_0 \psi_1 = E_1 \psi_1 \quad (17)$$

and ψ_2^- is an asymmetric nodal wave function (such as one lobe of a 2p hydrogenic function) defined by the step function

$$\psi_2^- = \begin{cases} \psi_2 & \text{for } z \leq 0 \\ 0 & \text{for } z \geq 0 \end{cases} \quad (18)$$

This function satisfies the eigenvalue equation in the limit as $W^- \rightarrow \infty$

$$H(W^- \rightarrow \infty) \psi_2^- = E_2 \psi_2^+ \quad (19)$$

The asymmetric nature of the wave function ψ_2^+ completely avoids the infinite asymmetric potential W^- so that there exists a bound surface state even though $W \rightarrow \infty$. A systematic investigation of the properties of allowed wave functions ψ_2^+ has already been carried out in Section I-B for the case of a Coulombic H_0 . The probability coefficients c_1 and c_2 are functions of W and will be calculated later.

There also exist antibonding surface states defined by the wave functions

$$\psi_u = c_1 \psi_1 + c_2 \psi_2^- \quad (20)$$

which by definition cannot avoid the wall repulsive potential and represent an energy E_u which approaches infinity as W does.

The expansion of ψ in Eq. (16) into two components represents only an approximation to the true wave function satisfying H . With particular choices of ψ_1 and ψ_2^+ , however, the hybrid energy states are practically correct near the limiting cases of $W = 0$ and $W = \infty$, respectively. In the intermediate case $0 < W < \infty$, the accuracy of the calculation can be improved by considering more functions of the ψ_1 and ψ_2^+ type. The gross idealization of the wall potential W^- , however, does not justify a more elaborate expansion than that given in Eq. (16). The ground state and all excited states of ψ will be considered in detail for a Coulombic H_0 in Section I-C-3.

2. Variational Calculation

To minimize E for arbitrary W the standard variational technique is applied to Eq. (13) yielding the set of relations:

$$(H_{11} - E) c_1 + (H_{12} - \Delta E) c_2 = 0 \quad (21a)$$

$$(H_{21} - \Delta E) c_1 + (H_{22} - E) c_2 = 0 \quad (21b)$$

where the normalization is, with $i, j = 1, 2$

$$\int \psi_i^* \psi_j d\tau = \begin{cases} 1 & \text{for } i = j \\ \Delta & \text{for } i \neq j \end{cases} \quad (22)$$

and the expectation value of the Hamiltonian is

$$H_{ij} = \int \psi_i^* (H_0 + W^-) \psi_j d\tau \quad (23)$$

such that

$$\begin{aligned} H_{11} &= E_1 + \frac{W}{2} \\ H_{22} &= E_2 \\ H_{12} &= H_{21} = \Delta E_1 \end{aligned} \quad (24)$$

Because of the unusual properties of the step functions ψ_2^+ and W^- , a few comments are necessary to show how the H_{ij} terms are derived. H_{11} is derived by using the eigenvalue equation for ψ_1 (Eq. 17); the coefficient 1/2 of W is necessary because W^- is nonzero only over half-space. H_{22} is *not* derived from an eigenvalue equation. Rather, H_{22} is merely the expectation value of H in the state of ψ_2^+ . The cross terms H_{12} and H_{21} are equal and are derived by operating with H on ψ_1 forwards and backwards, respectively, using Eqs. (17) and (22). If H is allowed to operate on ψ_2 , the same result is obtained, but with the complication of a nonvanishing delta function contribution at the origin due to the kinetic energy term $\nabla^2 \psi_2^+$.

To solve for the energy E it is convenient to introduce a dimensionless energy ϵ of the bound state E , and a dimensionless energy ω of the wall W , as follows:

$$\epsilon = \frac{(E - E_1)}{(E_2 - E_1)}, \quad \omega = \frac{W}{2(E_2 - E_1)} \quad (25)$$

Since all bound state energies E , E_1 , and E_2 are negative, the quantities $(E_2 - E_1)$ and $(E - E_1)$ are positive, so that ϵ and ω are positive. The secular determinant then becomes

$$\begin{vmatrix} \omega - \epsilon & -\Delta\epsilon \\ -\Delta\epsilon & 1 - \epsilon \end{vmatrix} = 0 \quad (26)$$

and the dimensionless binding energy is

$$\epsilon = \frac{\omega + 1 - \sqrt{(\omega - 1)^2 + 4\Delta^2 \omega}}{2(1 - \Delta^2)} \quad (27)$$

which is plotted as a function of ω in Fig. 4 for a selected particular value (Sect. I-C-3) of $\Delta = 0.296$. The figure shows that $\epsilon \sim \omega$ near $\omega = 0$ and that $\epsilon \rightarrow 1$ as $\omega \rightarrow \infty$. Actually, for $\omega = 2$, the dimensionless energy becomes $\epsilon = 0.94$ so that as far as the energy levels are concerned, an "infinite wall" occurs when $\omega > 2$.

The effect of gradually "turning on" the wall potential is seen to be a gradual raising of the energy levels of surface atom valence electrons. This effect actually occurs as evidenced by

the increase in free energy when a new surface is exposed. "Dangling electron bonds" can be visualized as hydrogen-like orbitals forced to occupy high energy states due to the surface asymmetry. Energy is released when symmetry is restored. These conclusions are independent of the precise forms of H_0 and W^- .

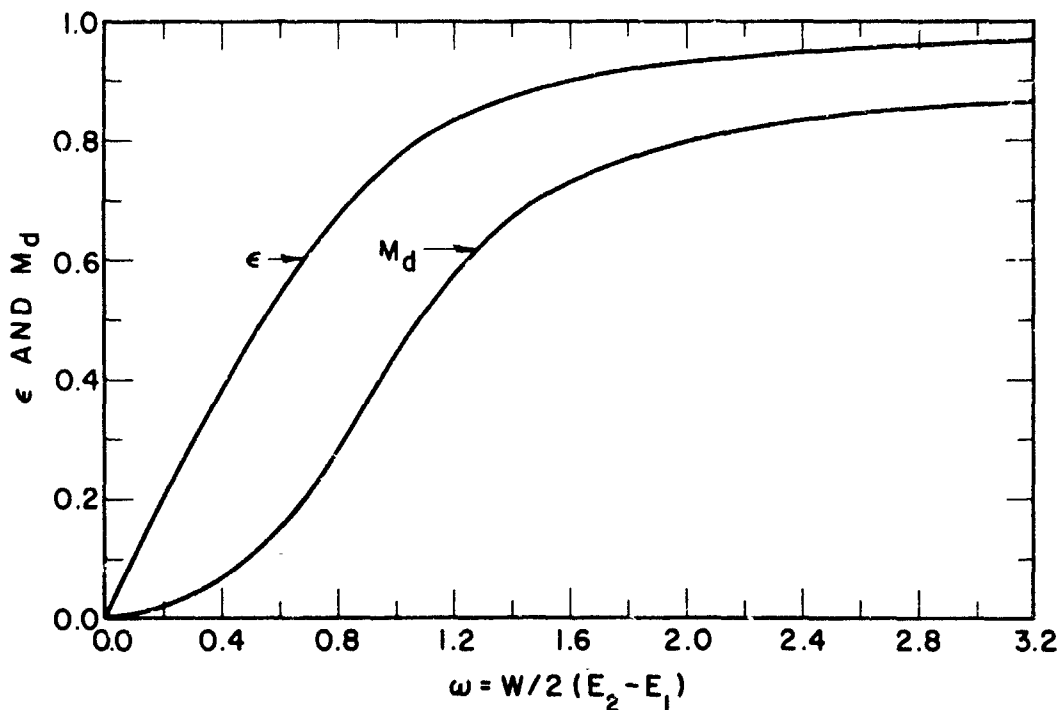


Fig. 4. Dimensionless energy ϵ and dipole moment M_d plotted versus dimensionless wall potential ω . As ω increases to infinity, ϵ and M_d both increase and approach unity.

By combining Eqs. (21) and (27) the wave function coefficients are calculated to be

$$c_1 = \frac{\epsilon \Lambda}{\sqrt{(1-\epsilon)^2 (1-\Lambda^2) + \Lambda^2}} \quad (28a)$$

$$c_2 = \frac{1-\epsilon}{\sqrt{(1-\epsilon)^2 (1-\Lambda^2) + \Lambda^2}} \quad (28b)$$

and are plotted as functions of ω in Fig. 5 for $\Lambda = 0.296$.

The changing valence bond character can be inferred from this figure using simple concepts of physical chemistry. The coefficient c_1^2 qualitatively represents the fraction of covalent character because ψ_1 is a symmetrical wave function characteristic of a covalent bond. The coefficient c_2^2 qualitatively represents the fraction of ionic character because ψ_2^+ is an asymmetric wave function characteristic of an ionic bond. Finally, the coefficient $2\Lambda c_1 c_2 = 1 - c_1^2 - c_2^2$ qualitatively represents the ionic-covalent resonance contribution to the bond character.

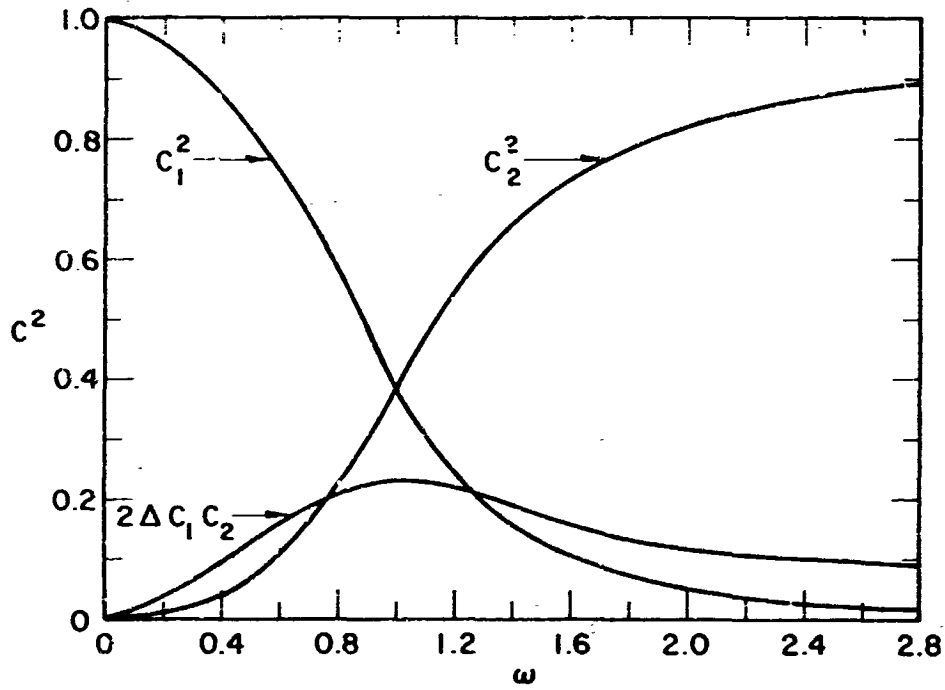


Fig. 5. Fractional bond character variation with wall potential.

c_1^2 = covalent fraction.

c_2^2 = ionic fraction.

$2c_1c_2\Delta$ = resonance fraction.

These coefficients are also useful for calculation of the surface dipole moment, $M = e \int \psi^* z \psi d\tau$, which, when expanded yields

$$M = e c_2^2 \int \psi_2^* z \psi_2 d\tau - 2e c_1 c_2 \int \psi_1^* z \psi_2 d\tau \quad (29)$$

An explicit calculation of M can be made if the functions ψ_1 and ψ_2 are reasonably estimated. One simple estimate of ψ_1 and ψ_2 can be made when H_0 is taken to be Coulombic as shown below.

3. Application to a Coulombic Hamiltonian

Many of the results of the preceding general treatment will become clearer if a particular single electron Hamiltonian H_0 is discussed in detail. For this purpose we choose a Coulombic Hamiltonian

$$H_0 = -\frac{\hbar^2 \nabla^2}{8\pi^2 \mu^*} - \frac{e^2}{\kappa r} \quad (30)$$

where μ^* is an effective electron mass and κ is a dielectric constant. Other Hamiltonians possessing bound states would yield qualitatively similar conclusions.

The eigenfunctions of $H_0 + W$ in the limit of $W \rightarrow 0$ are of the symmetric ψ_1 type and are labelled $\psi_{n\ell m}$ (r, θ, ϕ) where n , ℓ , and m are the usual hydrogenic quantum numbers. The spherical

coordinates r , θ , and ϕ are oriented such that the vector $\mu = 0$ points into the material and the plane $\theta = \pi/2$ lies in the surface plane. Energy levels E_n are given by

$$E_n = \frac{E_H \mu^2}{h^2 \kappa^2 \mu} \quad (31)$$

where E_H is the Bohr energy, 13.6 eV. Wave functions of a constant l subshell are $(2l+1)$ -fold degenerate, and of a constant n shell are $2n^2$ -fold degenerate, including spin up and down. Energy levels with fine splitting of the degenerate levels greatly exaggerated are shown at the *left* of Fig. 6 corresponding to $W = 0$. The three symbols labeling the levels refer to n , l , and m quantum numbers, respectively, and the notations m and \bar{m} refer to plus and minus z components of angular momentum.

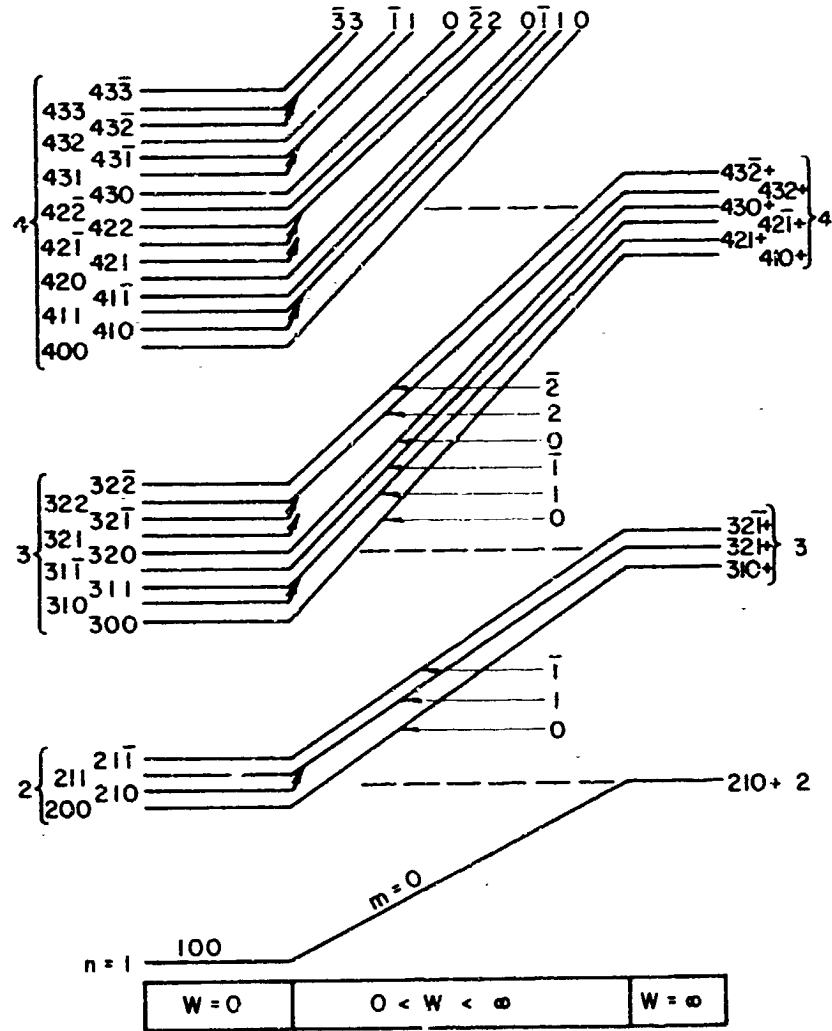


Fig. 6. Variation of Coulombic energy levels as the wall potential is turned on. Degeneracy of constant n shells is greatly exaggerated to show splitting into bonding states on the right side of the figure and antibonding states are shown as arrows pointing to the crystal continuum.

The binding eigenfunctions of $H_{\text{eff}} = W$ in the limit of $W \rightarrow \infty$ are of the asymmetric ψ_2 type and are labelled $\psi_{n',m}^-(r, \theta, \phi)$. These functions all vanish in the negative half plane $\pi/2 < \theta < \pi$ where the wall is located, and have planar nodes at $\theta = \pi/2$. The selection rule for planar nodes is $n' - m = \text{odd}$. It follows that wave functions of a constant n shell are 2 -fold degenerate, and of a constant n' shell are $n(n-1)$ fold degenerate, including spin-up and -down. Energy levels with exaggerated degeneracy are shown at the right of Fig. 6, corresponding to $W \rightarrow \infty$. There are, of course, an equal number of antibonding eigenfunctions labelled $\psi_{n',m}^+(r, \theta, \phi)$, but their energy levels blend into the material continuum and cannot be shown in Fig. 6.

To complete Fig. 6, the eigenfunctions ψ must be selected for an arbitrary W between the limits of 0 and ∞ . In accordance with Eq. (16) we select a linear combination of wave functions, one from the left of Fig. 6 and one from the right. Two plausible arguments point to a unique selection procedure. First, the presence of W which is axially symmetric cannot perturb the quantum number m , so connecting lines should be drawn with constant m . Second, it is most likely that states combine which have the same number of radial nodes. Thus, connecting lines should have constant $(n - n')$. Bound states are formed when $n - n'$ is odd:

$$\psi = c_1 \psi_{n-1, l-1, m}^- + c_2 \psi_{n', m}^+ \quad (32)$$

Using these rules, connecting lines in Fig. 6 indicate how the bound states vary in energy over the entire range of W . The small arrows in Fig. 6 indicate that an identical number of unbound states pass into the crystal continuum.

If this very simple scheme is observed, then all bound and unbound states are accounted for. As far as the bound states are concerned, the effect of the surface potential W is to increase the quantum numbers n and l by one unit each and thus to reduce the binding energy of the ground state and all excited states.

Illustrations of ψ as functions of W are schematically drawn in Fig. 7 for a few of the lowest states. At the left is the limit $W = 0$, at the right is the limit $W = \infty$, and in the center is an intermediate W . As W increases, the wave functions are forced into the interior of the material with no new radial nodes arising, like an elastic jelly. The elastic jelly is, in fact, a close mechanical analogy, since the presence of a free surface is known to increase the free energy of the material.

The energy and the dipole moment associated with each line in Fig. 6 for arbitrary W can be computed from Eqs. (27) and (29), provided κ , μ^*/μ , E_2 , E , and Δ are specified. As a particular example, consider the ground state composed of the normalized wave functions

$$\psi_{100} = \frac{e^{-r/a_0^*}}{\pi^{1/2}(a_0^*)^{3/2}} \quad (33)$$

$$\psi_{210}^+ = \frac{r \cos \theta e^{-r/2a_0^*}}{4\pi^{1/2}(a_0^*)^{5/2}} \quad (34)$$

where

$$a_0^* = \frac{\kappa \mu a_0}{\mu^*} \quad (35)$$

and a_0 is the first Bohr radius, 0.53 Å. The energy difference becomes $(E_2 - E_1) = (3/4) e^2 / 2ka_0^2$ and the overlap integral becomes $\Lambda = 0.296$. This value of Λ was used to construct Fig. 4.

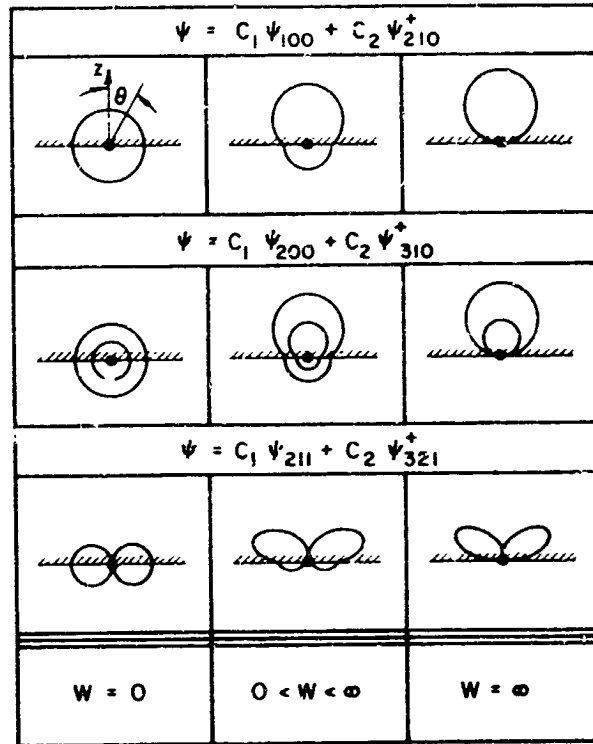


Fig. 7. Variation of three wave functions as the wall potential is turned on. Wall squeezes wave functions into the dielectric with no new radial nodes arising.

The above functions can also be used to explicitly calculate the dipole moment M_g of the ground state

$$M_g = \frac{15}{4} e a_0^* c_2^2 + \frac{256}{243} e a_0^* c_1 c_2 \Lambda \quad (36)$$

which can be expressed in conventional Debye units (10^{-18} esu-cm) as

$$M_g = \frac{\kappa \mu^*}{\mu} (9.54 c_2^2 + 0.79 c_1 c_2) \text{ Debyes} \quad (37)$$

It is convenient to define a dimensionless ground state dipole moment, $M_d = M_g / (9.54 \kappa \mu^* / \mu)$, which can also be plotted in Fig. 4 as a function of dimensionless wall energy ω .

Thus, the details of surface phenomena on dielectric materials can be explicitly calculated for ground states and also excited states without adjustable parameters.

4. Application to Cesium on Insulators

It is of interest to use the formalism developed here to compute the extent to which a surface cesium atom occupies a 1s or a 2p ground state. The criterion for whether the cesium will be in the 2p ground state is whether the wall potential is large compared to the binding energy. As seen from Fig. 2, the 2p state is essentially attained when $\omega \geq 2$.

To compute ω for cesium on sapphire estimate $\kappa = 9$ and $\mu/\mu^* = 1$. Then $E_1 = 13.6/9^2 = 0.168$ eV and $E_2 = E_1/4 = 0.042$ eV. The wall potential ω is essentially the electron affinity $\chi \approx 1$ eV. For cesium on sapphire, then

$$\omega = \frac{1}{2 \cdot (0.168 - 0.042)} = 4.0$$

so the ground state would essentially be a 2p nodal wave function with one lobe. A similar calculation shows similar results for alumina and glass substrates where $\kappa = 5-9$. The following calculations will therefore be based on 2p cesium wave functions for the surface ground state.

D. THEORY OF TUNNELING CONDUCTIVITY

Using the donor wave functions of Sections I-B and -C, it is possible to explicitly calculate electrical conductivity. The conductive mechanism considered here is electronic tunneling between surface donor atoms. Tunneling, hopping, and quantum mechanical resonance are all terms that will be used interchangeably to describe the same process.

Most of the derived equations contain only fundamental constants such as Planck's constant, unit electric charge, and electron mass. Other derived equations contain material constants such as ionic radius, interatomic spacing and atomic mass. The material constants are only necessary in the calculation of phonon energies. The approach taken here is unique in the sense that conductivity can be theoretically calculated *a priori*, without referring to conductivity data. Predictions made in this theoretical section agree very well with the experimental data as shown in later sections.

1. Tunneling Equation

Consider a line of donors on an insulator surface as schematically shown in Fig. 8a. Donor wave functions are of the 2p nodal type, penetrating into the insulator.

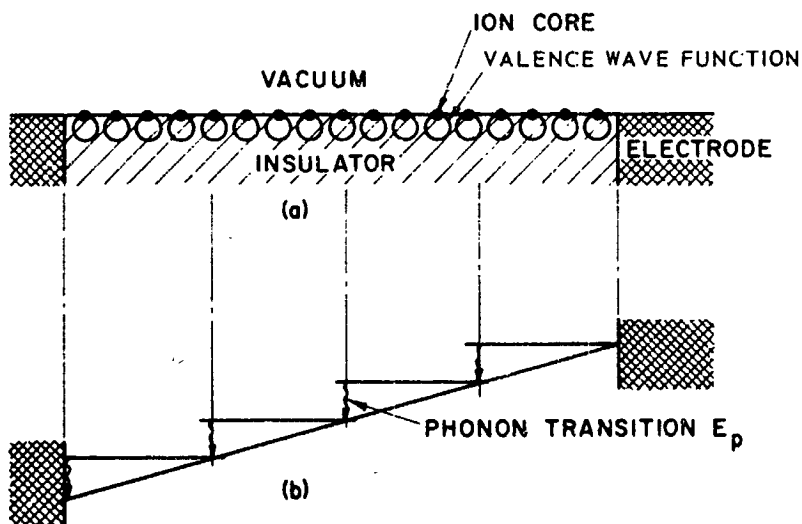


Fig. 8. Conduction due to a line of donor atoms on a surface.

- (a) Wave functions.
- (b) Energy states as a function of position. Wavy lines indicate phonon transitions which dissipate electrical energy.

In the absence of an applied electric field electrons can freely tunnel from one donor to another: electronic motion is random and isotropic. There is no drift current.

In the presence of an applied electric field a drift current must appear. This current is a small perturbation added to the random tunneling motion. At the present time, concepts of tunnel drift current are poorly understood. One very simple equation for tunnel drift current has been derived by Arnold and Patterson,¹⁴ but it has the conceptual weakness that it contains the thermal energy kT . Tunnel conductivity and field emission are quantum mechanical processes which should be temperature independent, to a first approximation.

The purpose of the derivation to follow is to modify the basic idea of Arnold and Patterson by essentially replacing kT by the lattice phonon energy E_p . The derived equation is still not rigorously true, but it has three advantages: it is very simple to apply to experimental data, it is temperature independent, and it rests on a more secure foundation than the equation of Arnold and Patterson.

To calculate the drift current between two adjacent donors in the field direction, the following relationship is useful:

$$(\text{drift current}) = (\text{random current}) \times (\text{drift probability}) \quad (38)$$

The random current can be written as

$$(\text{random current}) = eE_t/h \quad (39)$$

where e is the unit electric charge, E_t is the tunneling energy (dependent on donor spacing) and h is Planck's constant. The ratio E_t/h is the frequency of random tunneling.

The drift probability is a more difficult concept to apply.¹⁴ If one recognizes that all electrons in the drift current eventually dissipate energy, then the drift probability should nearly equal the energy dissipation probability, so that

$$(\text{drift probability}) = eV_a/E_p \quad (40)$$

where eV_a is the potential energy acquired between adjacent donors, and E_p is the phonon energy which is responsible for energy dissipation in quantum processes. Arnold and Patterson (erroneously) used kT instead of E_p in the above expression. The term V_a is normally very small ($\sim 10^{-6}$ V), being equal to the applied voltage (normally ~ 1 V) divided by the number of donors in a line (normally $\sim 10^6$). Since E_p is normally $\sim 10^{-2}$ eV, the drift probability is normally calculated to be $\sim 10^{-4}$. Two important limiting cases arise: when eV_a vanishes, the drift vanishes; and when eV_a equals E_p , each tunneling electron liberates a phonon to the substrate lattice. The production of phonons is indicated by the wavy lines in Fig. 8b. In essence, the phonon transitions act as mechanical ratchets since they restrict electrons to drift only in one direction.

By combining Eqs. (38)-(40) the interatom drift current becomes

$$i_a = \frac{e^2 E_t V_a}{h E_p} \quad (41)$$

The interatom conductivity is then given by

$$g_a = \frac{i_a}{V_a} = \frac{e^2 E_t}{h E_p} \quad (42)$$

Note that g_a is Ohmic (i.e., g_a is independent of V_a). If a square lattice of donors is assumed, then g_a equals the conductivity per square g_{\square} . The desired relationship between the measurable quantity g_{\square} and the atomic parameters E_t and E_p is therefore

$$g_{\square} = \frac{e^2 E_t}{h E_p} \quad (43)$$

or

$$g_{\square} = 0.385 \times 10^{-4} E_t/E_p \text{ mhos/square} \quad (44)$$

It should be recognized that the hypothetical square lattice of surface donors is not related to the substrate lattice at all; instead, the donor lattice varies continuously as the donor coverage varies. The donor lattice merely expresses the idea that interdonor repulsive forces are effective in establishing a more uniform distribution of donors than if the donors were in the random positions.

Explicit calculations of the tunneling and phonon energies, E_t and E_p , are given below. Note that e^2/h is a fundamental constant having the dimensions of conductivity.

2. Tunneling Energy

The simplest and most carefully studied system exhibiting electron tunneling^{14,15} is the hydrogen molecule ion H_2^+ . The single electron can be located either about one nucleus or the other, but because each of the locations is equally probable, the electron resonates, or tunnels, between the two nuclei. The tunneling frequency ν_t associated with the process has an associated tunneling energy E_t given by $E_t = h\nu_t$. For H_2^+ , the tunneling energy (also called the exchange or resonant energy) is given by

$$E_t = \frac{-e^2}{\kappa} \int \frac{\psi^*(r) \psi(L-r)}{r} d^3r \quad (45)$$

where $\psi^*(r)$ and $\psi(L-r)$ are 1s hydrogenic wave functions centered about locations 0 and L, respectively. Essentially, E_t is the Coulomb energy $e^2/\kappa r$ averaged over the resonant wave function probability, $\psi(r) \psi(L-r)$.

Arnold and Patterson¹⁴ have used Eq. (45) to successfully explain certain tunneling phenomena in alkali-ammonia solutions. In particular, they incorporated 1s hydrogenic ground states for the alkali atoms.

To use Eq. (45) in surface tunneling phenomena the wave functions in the ground state must be of the 2p type. Tunneling integrals of two atoms with parallel 2p wave functions have fortunately been explicitly calculated by Kopineck.^{16,17} The molecular designation of the overlap is called $\pi-\pi$ overlap, meaning that one nodal plane passes through the two nuclei. Because of

this nodal plane. Kopineck's tunneling integral, which he calls $J_{\pi\pi}$, is identical to twice his integral taken over only one half-plane. But since the ground state surface wave functions have a $\sqrt{2}$ normalization (Section I-B-2), Kopineck's $J_{\pi\pi}$ is fortunately equal to the surface tunneling energy of Eq. (45). This allows Eq. (45) to be written in expanded form as

$$E_t = \frac{-e^2 a^2 \exp(-a)}{12\kappa^2 a_o^*} \left[1 + \frac{3}{a} + \frac{3}{a^2} \right] \quad (46)$$

Here a is a dimensionless interdonor spacing parameter, dependent on donor coverage. To be precise, a is defined as

$$a = \frac{L\mu^*}{2\kappa a_o \mu} \quad (47)$$

where L is the interdonor spacing, κ is the dielectric constant, a_o is the first Bohr radius, and μ^*/μ is the ratio of effective to free electron mass.

If a square lattice of surface donors is assumed (see part II-D-1), then L has a simple relationship to the donor surface coverage. The relationship follows because the density of donors per unit surface area can be written in two ways which are equated to obtain

$$\sigma\theta = \frac{1}{L^2} \quad (48)$$

Here σ is the surface density at one monolayer and θ is the fractional coverage. Equation (48) has been quoted by deBoer,¹⁸ Topping,¹⁹ and many others for square adsorbate lattices; also, a minor variation of Eq. (48) has been used by Langmuir²⁰ for hexagonal adsorbate lattices.

The relationship between the dimensionless spacing a and the coverage θ is obtained by combining Eqs. (47) and (48):

$$\frac{1}{a^2} = (4\sigma a_o^2) \kappa^2 \left(\frac{\mu}{\mu^*} \right)^2 \theta \quad (49)$$

If σ is taken equal to $4.8 \times 10^{14} \text{ cm}^{-2}$ (characteristic of cesium at one tightly packed monolayer)²¹ then the first bracketed coefficient in Eq. (49) is equal to 0.0054. Note that θ is proportional to a^{-2} .

With this information it is instructive to carefully examine the variation of tunneling energy with coverage. To eliminate e^2 , κ , a_o , and (μ^*/μ) from the discussion it is convenient to normalize the tunneling energy E_t by dividing it by the ionization energy E_i of Eq. (10). After rearrangement Eq. (46) becomes

$$\frac{E_t}{8E_i} = \frac{a^2 \exp(-a)}{12} \left(1 + \frac{3}{a} + \frac{3}{a^2} \right) \quad (50)$$

The above equation is arranged with foresight such that the right-hand side is precisely Kopineck's tunneling integral which he tabulated from $a = 0.5$ to $a = 7.0$. We have extended the range from $a = 7.0$ to $a = 12.0$. It is thus possible to plot E_t/E_i as a universal function of the dimensionless parameter a .

A more conventional plot, however, can be constructed in the following way recognizing that θ is proportional to a^{-2} . This plot is shown in Fig. 9. Here the ordinate, E_t/E_i , is proportional to the tunneling energy; and the abscissa, a^{-2} , is proportional to the coverage of surface

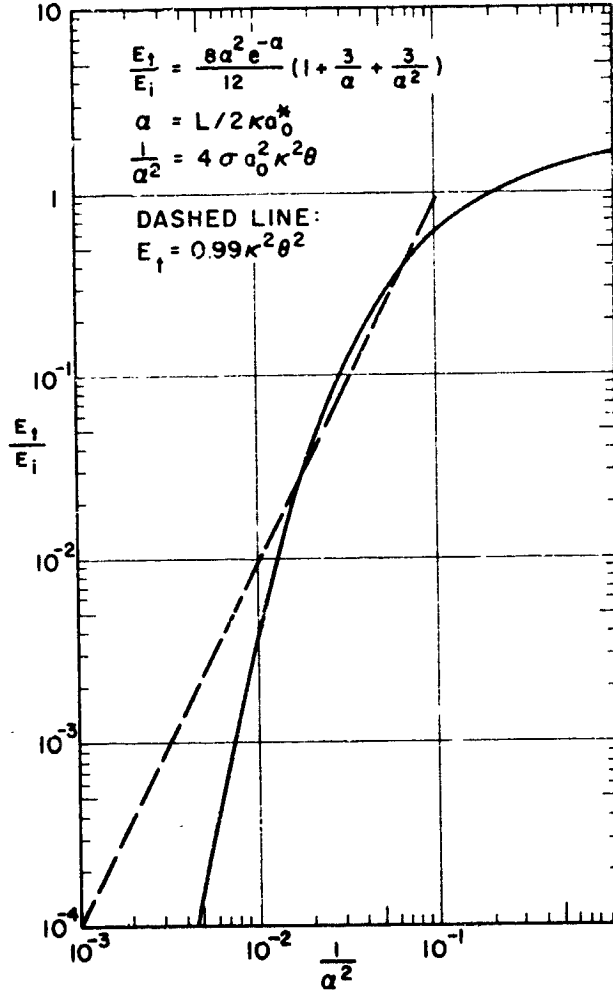


Fig. 9. Dimensionless tunneling energy versus a^{-2} , which is proportional to coverage. The dashed line is an adequate approximation for a large range of E_t/E_i .

donors. The curve on this graph is universal, being independent of κ and μ^*/μ . Four conclusions emerge from examining this plot:

(1) $E_t/E_i > 1$ at high coverages, indicating that there is more electron delocalization than electron localization. Conductivity is metallic and traveling Bloch waves of the form $\exp(ikr)$ carry electronic current. This case is not of primary interest for the discussion to follow.

(2) $E_t/E_i < 1$ at low coverages, indicating that electrons are mainly localized but that tunneling can occur to a limited extent. Conductivity occurs by quantum mechanical hops, not by continuous Bloch waves. The situation is analogous to tunneling conductivity in alkali-ammonia solutions.¹⁴

(3) Near $E_t/E_i = 1$ a critical transition from metallic to tunneling conductivity should occur. The critical spacing ratio is approximately

$$a_c = \sqrt{10} \quad (51)$$

(4) In the tunneling range the dashed line is a fair approximation to the computed solid line. The equation for the dashed line, assuming $\mu = \mu^*$, is

$$\frac{E_t}{E_i} = 100 a^{-4} - 0.289 \kappa^4 \theta^2 \quad (52)$$

showing that E_t is proportional to the coverage squared. In the very low coverage range the dashed line departs from the solid line. It is surprising that all data to be described in Sections I-F and -G seem to fit the dashed line more accurately. Reasons for this effect are not clear. The dashed line is extremely simple to manipulate algebraically and will be used in the analysis to follow.

This completes the calculation of the tunneling energy and its dependence on coverage, dielectric constant, and effective mass. Admittedly, many simplifications are used in the derivation. Probably the most serious omission is the neglect of many particle interactions. Nevertheless, this simplified treatment of only two body interactions is, in fact, fairly accurate as judged by experimental data.

3. Phonon Energy

Energy introduced into a conductor by an electric field will eventually be dissipated either by photons or phonons. Photon energy transitions are proportional to the cube of the transition energy, so that they are generally rare compared to low-energy phonon transitions.

Phonon energies of an isotropic solid follow the Debye distribution to a first approximation with a characteristic bulk phonon energy E_B and Debye temperature θ_D related by

$$E_B = k\theta_D \quad (53)$$

where k is Boltzmann's constant. But an adsorbed surface atom has a mean phonon energy E_p different from that of the bulk value. This energy is given by one vibrational quantum and is related to the vibrational frequency ν_p by

$$E_p = h\nu_p \quad (54)$$

A simple procedure for calculating ν_p for any adsorbed species on a surface has been given in detail by the author²² and is summarized below.

Consider a cesium ion located on a sapphire surface. Sapphire is crystalline Al_2O_3 consisting of O^{2-} ions placed on a hexagonal close-spaced lattice with Al^{+++} ions placed in the interstices. A cesium ion will most probably be nestled on top of three oxygen ions arranged on vertices of an equilateral triangle as shown in Fig. 10. The cesium will undergo vibrations

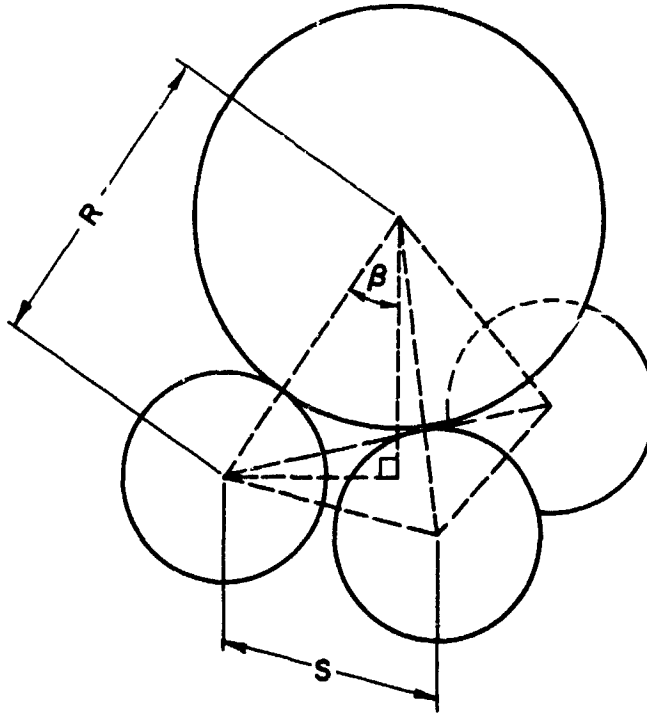


Fig. 10. Pyramidal molecule consisting of one cesium ion nestled on top of three oxygen ions. Phonons are transferred via the vertical molecular vibrations.

perpendicular to the surface with frequency ν_p which will now be calculated from a harmonic oscillator model. The equation²² is

$$\nu_p = \frac{1}{2\pi} \sqrt{\frac{2\phi_a}{\bar{m}}} \frac{1}{R \cos \beta} \quad (55)$$

where ϕ_a is the heat of adsorption, \bar{m} is the reduced mass of the pyramidal molecule, R is the sum of ionic radii of cesium and oxygen, β is half the apex angle, and s is the interoxygen spacing.

Typical values of these parameters are

$$\phi_a = 0.9 \text{ eV}$$

$$\bar{m} = \frac{3m_{cs}m_o}{m_{cs} + 3m_o} = 35$$

$$R = r_{cs}^+ + r_o^- = 3.05 \text{ \AA}$$

$$\cos \beta = (1 - S^2/3R^2)^{1/2} = 0.88$$

$$s = 2.50 \text{ \AA}$$

which gives

$$\nu_p = 0.97 \times 10^{12} \text{ sec}^{-1}$$

and

$$E_p = 0.0040 \text{ eV}$$

(56)

These results are insensitive to ϕ_a and \bar{m} because of the square root dependence. In the discussion to follow, Eq. (56) will be compared with experimental data in the absence of other information regarding the surface structure of alumina polycrystalline ceramics or glass.

4. Parametric Analysis

By combining Eqs. (44) and (46) the conductivity becomes a unique function of θ :

$$g_{\square} = \frac{e^4 a^2 \exp(-a)}{12 h \kappa^2 a_o^* E_p} \left(\frac{1}{a} + \frac{3}{a} + \frac{3}{a^2} \right) \quad (57a)$$

In particular, by using the straight-line approximation of Eq. (52) and the phonon energy of Eq. (66), one gets

$$g_{\square} = b\theta^2 \quad (57b)$$

$$b = 0.0094 \kappa^2 \text{ mhos/square}$$

which is plotted on a log-log scale in Fig. 11. The dielectric constant κ is a running parameter allowed to vary from 1 to 100.

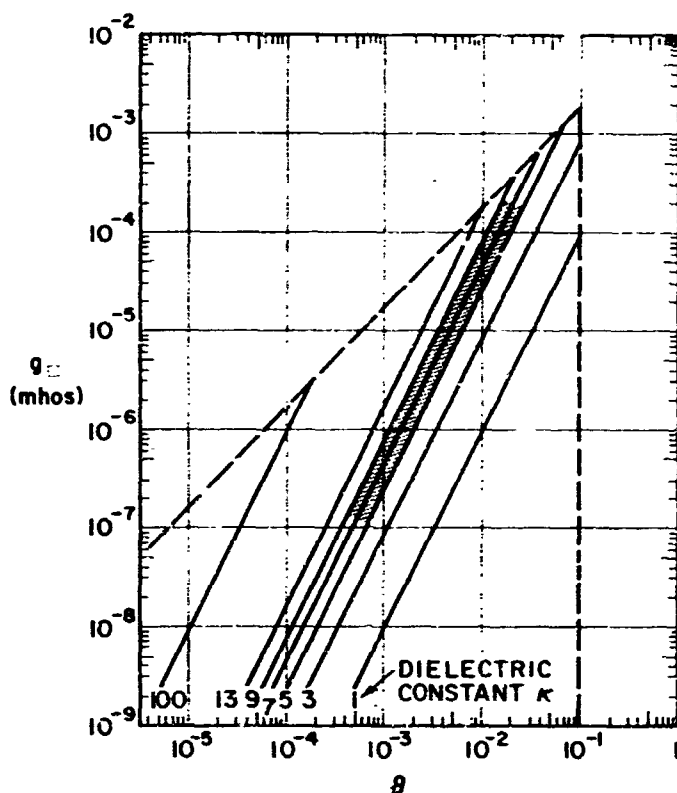


Fig. 11. Parametric theoretical plot of tunneling conductivity versus coverage for various values of dielectric constant. Shaded area indicates region where data have been obtained.

The figure consists of a family of straight lines, one line for each κ value. The region to the upper left bounded by a dashed line is not applicable since $E_t > E_i$ and metallic conductivity occurs there. The region to the right bounded by a vertical dashed line is not applicable since the coverage is too high, $\theta > 0.1$, and cooperative interadsorbate effects tend to dominate. In particular, the heat of adsorption is expected to be constant only for $\theta < 0.1$. Data have been taken in the shaded region of the figure.

More information regarding the range of meaningful κ values can be obtained from Table I. Small κ values, $\kappa < 3$, are questionable since the theory of nodal wave functions was based on dielectric constants significantly greater than unity. Large κ values ($\kappa > 11$) are questionable since $kT_{room} > E_i$, and the states are most probably thermally ionized into the conduction band. The theory seems to apply best to intermediate κ values in the range $3 < \kappa < 11$.

Another restriction is that of small overlap: The mean lateral radius \bar{r} should be less than one-half the mean lattice spacing L . With \bar{r} defined by

TABLE I
THEORETICALLY CALCULATED PROPERTIES IMPORTANT TO SURFACE TUNNELING

κ	E_i (eV)	r (Å)	L_s (Å)	θ	g (mho)	$b = g/\mu^2$
DIELECTRIC CONSTANT	IONIZATION ENERGY	MEAN LATERAL RADIUS	SMALLEST SPACING	LARGEST COVERAGE	LARGEST TUNNELING CONDUCTIVITY	
1	3.4	1.6	14	0.10	$1.0 \cdot 10^{-4}$	0.0094
3	0.38	1.7	14	0.10	$8.0 \cdot 10^{-4}$	0.085
5	0.14	1.8	17	0.074	$13 \cdot 10^{-4}$	0.23
7	0.069	11	23	0.038	$6.7 \cdot 10^{-4}$	0.46
9	0.042	14	30	0.023	$4.0 \cdot 10^{-4}$	0.76
11	0.028	17	37	0.015	$2.7 \cdot 10^{-4}$	1.14
13	0.020	20	44	0.009	$1.9 \cdot 10^{-4}$	1.59
100	0.0003	156			$0.033 \cdot 10^{-4}$	94

$$\bar{r} = \int \psi^* \sqrt{x^2 + y^2} \psi \, d\tau / \int \psi^* \psi \, d\tau \quad (58)$$

calculation shows that

$$\bar{r} = (15-16) \pi \kappa a_0^* \quad (59)$$

for the 2p ground state. Values of \bar{r} , assuming $\mu^* = \mu$, and the smallest meaningful internuclear spacing L_s from Fig. 11 and Eqs. (48, 49 and 51) are both shown in Table I; the small tunneling overlap condition is indeed observed for all κ considered.

The largest allowable coverage in the valid κ range varies from $0.01 < \theta < 0.1$ showing that the surface donors are indeed dilute as implicitly assumed in the derivation of wave functions of individual adatoms.

Finally, Table I shows that in the allowed κ range, tunneling conductivity should not exceed $\sim 10^{-3}$ mhos/square. If surface conductivity is observed greater than this theoretical value, then one can infer the conduction mechanism to be metallic and rather insensitive to the concentration of surface donors. The transition from tunneling to metallic conductivity has been observed in alkali-ammonia solutions.¹⁴ For surface conductivity, bulk condensation occurs before the transition has a chance to appear.^{1, 2}

In summary, the theoretical analysis of this section shows that tunneling conductivity can be explicitly calculated without any reference to experimental data. Tunneling conductivity occurs in dilute surface layers, $\theta < 0.1$, and it varies approximately as θ^2 .

In dynamic equilibrium the coverage θ is a function of surface and metallic vapor bath temperatures. This functional dependence is derived in the following section.

E. EQUATION OF STATE

To calculate the coverage θ of surface donors consider a surface at temperature T immersed in a metallic vapor bath at temperature T' . Provided $T \sim T'$, dynamic equilibrium is

established and agglomeration of the adsorbate donor atoms into crystallites is thermodynamically unstable. There will exist a two-dimensional adsorbate donor gas which is constantly agitated due to rearrangement, adsorption, and desorption.

The equation of state relating θ to T and T' is extremely simple at low coverages, $\theta < 0.1$, because the heat of adsorption is then largely independent²⁴ of coverage and temperature. The equation of state constructed from a rate balance is²²

$$\omega \nu_p \sigma \theta e^{\Delta s/k} e^{-\phi_a/kT} = \omega' \nu' \sigma' e^{-\phi'/kT} \quad (60)$$

where ω = surface statistical weight
 ν_p = surface vibrational frequency
 σ = surface monolayer density
 θ = surface coverage
 Δs = surface configurational entropy
 ϕ_a = surface adsorption heat
 T = surface temperature
 ω' = liquid statistical weight
 ν' = liquid vibrational frequency
 σ' = liquid monolayer density
 ϕ' = liquid vaporization heat
 T' = liquid temperature
 k = Boltzmann's constant

This equation is based on the model of a mobile two-dimensional layer with one degree of vibrational freedom perpendicular to the surface. The surface statistical weight ω is considered only for the lowest electronic state of the donor atom. Departures either from the model or in the restriction to ground state statistical weights will be taken up, at least approximately, in the configurational entropy term $\Delta s/k$. Neither $\Delta s/k$ nor ϕ_a can be predicted from more fundamental ideas at the present time. They will be inferred from experimental data later on. Close estimates of the other parameters²² can be made, however, and are listed below for cesium on insulators.

$$\begin{aligned} \omega &= 2 \\ \omega' &= 1 \\ \nu_p &= 0.97 \times 10^{12} \text{ sec}^{-1} \\ \nu' &= 1.26 \times 10^{12} \text{ sec}^{-1} \\ \sigma &= 4.8 \times 10^{14} \text{ cm}^{-2} \\ \sigma' &= 4.16 \times 10^{14} \text{ cm}^{-2} \\ \phi' &= 0.747 \text{ eV} \end{aligned}$$

On the insulator surface, cesium donor electron spins are probably uncorrelated in the dilute case; the electronic statistical weight for the ground state is then $\omega = 2$. On the cesium liquid, the spins are always paired so that $\omega = 1$. Using these values Eq. (60) becomes

$$\theta = 0.545 e^{-\Delta s/k} e^{-\phi/kT'} e^{\phi_a/kT} \quad (61)$$

By combining this equation of state with the general conductivity relation [Eq. (57a)] the following general theoretical predictions result:

1. Since $\log \theta$ is a single-valued function of $1/T$ and $1/T'$ and since g_{\square} is a single-valued function of θ , it follows that $\log g_{\square}$ should be a single-valued function of $1/T$ and $1/T'$. This dependence can be visualized most easily by imagining a plot constructed with $1000/T$ as ordinate and $1000/T'$ as abscissa. It follows that on this plot lines of constant g_{\square} would never intersect.
2. The slope of this plot, being defined by

$$\text{slope} = \left. \frac{\partial (1000/T)}{\partial (1000/T')} \right|_{\text{constant } g_{\square}}$$

is theoretically calculated to be ϕ'/ϕ_a and constant, provided θ is sufficiently low so that ϕ_a is coverage- and temperature-independent.

3. The horizontal spacing of g_{\square} lines differing by constant factors, say factors of 10, will generally vary.

In summary, general considerations indicate a family of nonintersecting, parallel, and non-uniformly spaced lines of constant conductivity on a $1000/T$, $1000/T'$ plot.

In addition to these general predictions, more specific predictions can be drawn if the conductivity can be written in the power law form

$$g_{\square} = b\theta^{\gamma} \quad (62)$$

where γ is any power of θ . Then the lines of constant g_{\square} will be equally spaced.

For the particular case when the straight-line approximation of Eq. (57b) is assumed, $\gamma = 2$ and lines of constant g_{\square} such as $g_{\square} = 10^{-4}, 10^{-5}, 10^{-6}, 10^{-7}$, etc., would be equally spaced $2 \times 0.745/5.05 = 0.295$ units apart on the horizontal axis $1000/T'$. The conductivity can then be written in closed form as

$$g_{\square} = b\theta^2 = 0.297 b e^{-2\Delta s/k} e^{-2\phi'/kT'} e^{2\phi_a/kT} \quad (63)$$

To compare theory with experimental data it is convenient to use the Arrhenius form

$$\text{Log}_{10} g_{\square} = A - \frac{B}{T'} + \frac{C}{T} \quad (64)$$

where

$$\left\{ \begin{array}{l} A = -0.52 + \text{Log}_{10} b - 0.85 \Delta s/k \\ B = 2 \times 5050 \times \phi = 7550 \\ C = 2 \times 5050 \times \phi_a = 10,100 \phi_a \end{array} \right\} \quad (65)$$

The theoretical constant B is rigidly fixed, while the constants A and C contain the configurational entropy and heat of desorption, respectively, which will be inferred by comparison with data taken under "clean" experimental conditions.

If the effect of contaminants would be merely to alter γ , then an Arrhenius equation would still occur, but with A, B, and C values different from Eq. (65). The slopes B/C of the g_{\square} line family would, however, be unaltered and the line spacings would still be uniform.

Analysis of the Arrhenius equations provides a very sensitive probe to determine the extent of adsorbate and contaminant gas interaction. Data reported below will serve to display various predicted effects occurring under "clean" and "unclean" conditions.

F. ELECTRICAL CONDUCTIVITY CAUSED BY ADSORBED CESIUM ON INSULATOR SURFACES*

ABSTRACT

Electrical conductivity caused by adsorbed cesium on various insulator surfaces has been measured extensively. The insulators used were high alumina "Diamonite" ceramic, high alumina "Frenchtown" ceramic, and pure crystalline sapphire; the surface temperatures varied in the range $300^{\circ}\text{K} < T < 600^{\circ}\text{K}$; the cesium vapor bath temperatures varied in the range $300^{\circ}\text{K} < T' < 500^{\circ}\text{K}$; and data were taken both with and without a continuously purifying cesium still and getter ion pump. It was found that:

1. The conductivity per square, g_{\square} , is surprisingly reproducible and identical for all high alumina substrates, provided either vapor contaminants are continuously gettered or an isolated system is in early stages of life, and follows a semiempirical law over many orders of magnitude

$$\text{Log}_{10} g_{\square} = A - \frac{B}{T'} + \frac{C}{T} \text{ (mho)} \quad (66)$$

where $A = -5.4$, $B = 7520$, and $C = 8340$.

2. For isolated systems in later stages of life where unknown contaminant gases accumulated, the conductivity is again reproducible but higher with entirely different values of $A = -4.5$, $B = 2400$, and $C = 2700$.

These data may be applied to choosing insulators for thermionic energy converters and associated test devices.

G. COMPARISON OF THEORY WITH EXPERIMENT

Experimental data of electrical conductivity caused by adsorbed cesium on insulators has already accumulated (see Section I-F and References 1-3). It is necessary first to present the data in a compact form so that it can be neatly compared with theory.

The conductivity of cesium on all "clean" alumina (including sapphire) systems follows the theoretical Arrhenius relationship [Eq. (64)] with A, B, and C values given by²

$$\left. \begin{array}{l} A = -5.4 \\ B = 7520 \\ C = 8340 \end{array} \right\} \text{ "clean" alumina} \quad (67)$$

* This work was reported in its entirety in the *Proceedings of the Thermionic Specialist Conference*, Cleveland, Ohio, October 1964, and is summarized here.

The data are shown in Fig. 12. "Clean" conditions are defined as continuously gettered systems at low temperatures and in initial stages of life.

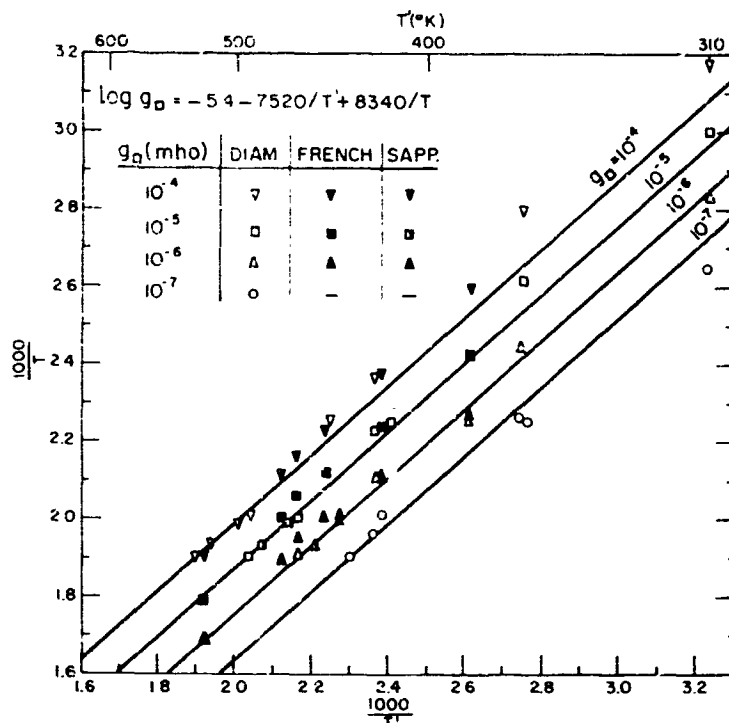


Fig. 12. Master plot of constant conductivity versus reciprocal bath and surface temperatures, taken under "clean" conditions. Data refer to Diamonite ceramic, Frenchtown ceramic, and sapphire. Lines follow semiempirical Arrhenius formula.

Blackford³ reported conductivity data for cesium on "clean" Pyrex glass surfaces. His data yielded

$$\left. \begin{array}{l} A = -6.6 \\ B = 7520 \\ C = 8340 \end{array} \right\} \text{"clean" Pyrex} \quad (68)$$

as shown in Fig. 13.

Finally, for "unclean" alumina systems the Arrhenius parameters representing the data became²

$$\left. \begin{array}{l} A = -4.5 \\ B = 2400 \\ C = 2700 \end{array} \right\} \text{"unclean" alumina} \quad (69)$$

The data are shown in Fig. 14. "Unclean" conditions are defined as pinched off and nongettered systems where residual gases have a chance to accumulate.

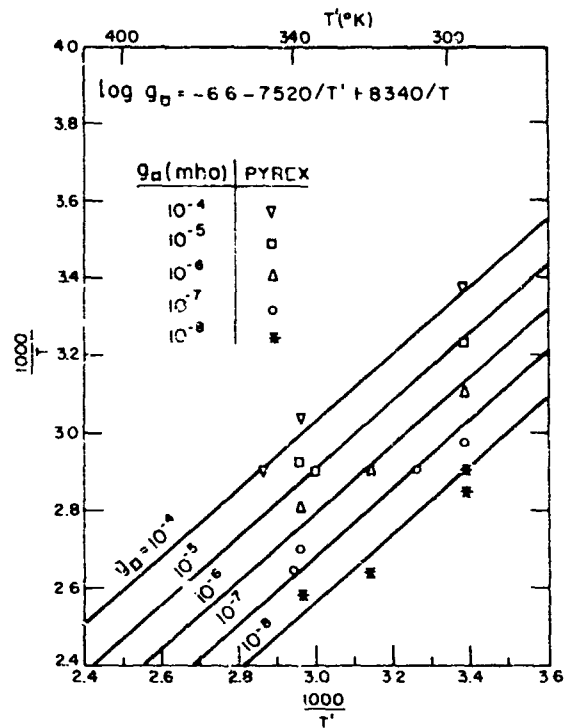


Fig. 13. Master plot of Blackford's cesium on Pyrex glass data. The semiempirical line formula is similar to that of cesium on ceramic under "clean" conditions.

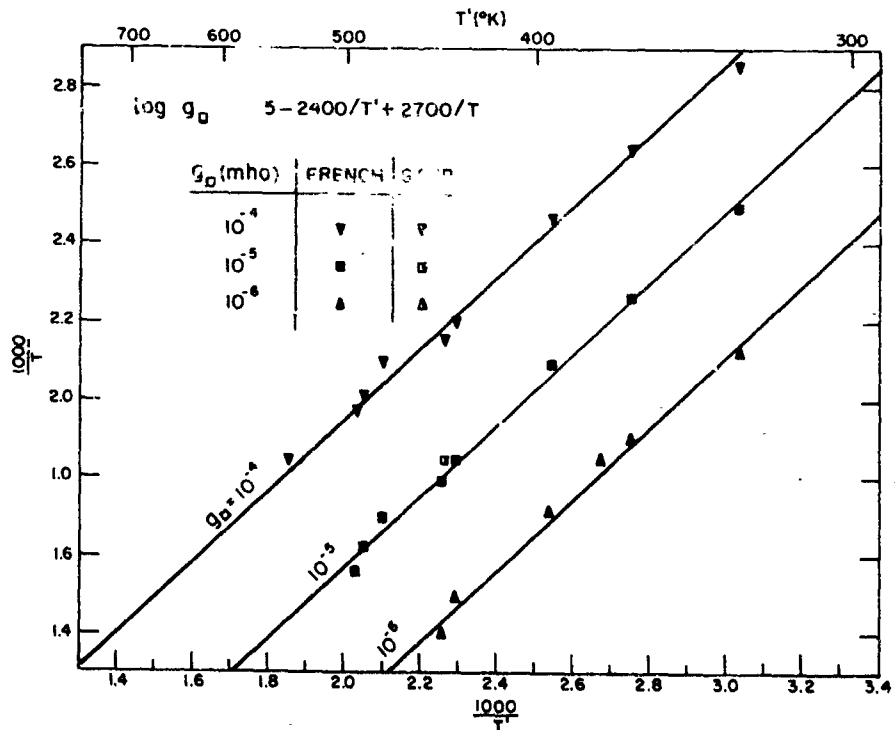


Fig. 14. Master plot of constant conductivity versus reciprocal bath and surface temperatures, taken under "unclean" conditions.

The transition between "clean" and "unclean" alumina systems was followed after a getter ion pump was pinched off. There is a gradual transition such that A, B, and C values slowly change from Eq. (67) to Eq. (69). After about one week of constant testing a final equilibrium is attained which allowed the determination of Eq. (69).

Let us now interpret all the data in terms of the theoretical predictions set forth in Section I-E.

The fact that the data always follow Arrhenius conductivity relationships indicates that:

- (a) Conductivity follows a power law of coverage given by

$$g_{\infty} = b\theta^v \quad (70)$$

- (b) Line slopes are identical.
 (c) The observed conductivity is not a sum of partial conductivities because the Arrhenius relationship is inconsistent with a sum of effects.
 (d) The conduction mechanisms on glass and crystalline sapphire are similar, confirming the prediction of surface electron tunneling proposed in Section I-D.

The fact that for clean systems the theoretical B value (7520) and the experimental B values *exactly agree* shows that the conductivity is proportional to the coverage squared as theoretically anticipated.

For unclean systems the experimental B value is 1/3 of the theoretical value; this indicates that the contaminant causes the conductivity to vary as the coverage to the two-thirds power. The contaminant gas, most probably hydrogen,² is deduced to *aid* the tunneling between cesium atoms and to increase the conductivity. Possibly the hydrogen acts as a bridge for the cesium-cesium tunneling process.

For clean systems, comparison between theoretical and experimental C values shows that

$$\phi_a = 0.83 \text{ eV} \quad (71)$$

which is 0.08 eV higher than the vaporization heat of bulk cesium ($\phi' = 0.75 \text{ eV}$). An independent check of ϕ_a was made in the following simple experiment.* A mass of fine alumina powder was painted on one electrode in an evacuated glass tube containing liquid cesium droplets. At constant temperature it was discovered that the droplets spontaneously became smaller, and the cesium gradually appeared in the alumina powder as judged from its color progression: white to blue to black. As soon as the powder was warmed to about 100°C, however, the cesium departed the powder and became redeposited in liquid droplets on the glass walls. The observed 100°C temperature difference required to reversibly transport cesium from the powder to the droplets indicates that ϕ_a and ϕ' are fairly close. The observed fact that at constant temperature, cesium prefers the adsorbed state to the cesium droplet state indicates that ϕ_a is slightly greater than ϕ' . Thus, this experiment helps to verify the calculated ϕ_a value deduced above. For both clean and unclean systems the ratio B/C is constant, indicating that ϕ_a is constant and unperturbed by contaminants.

* K. G. Hernqvist, RCA Laboratories, unpublished data.

For clean alumina the theoretical A value can be calculated provided κ , μ^*/μ , and $\Delta s/k$ are known. Inserting reasonable values of $\kappa = 9$ and $\mu^*/\mu = 1$ into Eq. (65) yields $A = -0.64 - 0.87 \Delta s/k$. By comparing this with the experimental A value of -5.4 , the configurational entropy change is calculated to be

$$\Delta s/k = 5.5 \quad (72)$$

Similarly, assuming $\kappa = 5$ and $\mu^*/\mu = 1$ for clean Pyrex one obtains

$$\Delta s/k = 6.2 \quad (73)$$

$\Delta s/k$ values are dependent on the adsorption model as well as the parameters κ and μ^*/μ . Their large magnitudes indicate²² a reduction in translational freedom, possibly arising from an ordering due to dipole-dipole repulsions. This interpretation is in agreement with the long-range ordering observed in many low-energy electron diffraction (LEED) experiments. It also follows that if a fixed, long-range order is assumed, then $\Delta s/k$ should be fixed, and the absolute value of A should increase with decreased dielectric constant [see Eqs. (65) and (57b)]. This theoretically predicted trend has indeed been observed experimentally: for alumina, $\kappa \approx 9$ and $A = -5.4$; and for Pyrex, $\kappa \approx 5$ and $A = -6.6$.

H. CONCLUSIONS DRAWN FROM CESIUM ADSORPTION ON INSULATORS

Starting from fundamental quantum mechanical concepts, it has been possible to theoretically derive wave functions, donor ionization energies, tunneling energies, conductivity relationships, and equations of state, all in excellent agreement with the extensive experimental data taken to date.

Some of the highlights of this effort are:

1. The ground state wave function of a cesium atom on a dielectric surface consists of one lobe of a $2p$ hydrogenic wave function penetrating deep into the dielectric.
2. General rules for selecting surface wave functions of all excited states and arbitrary surface asymmetry have been derived.
3. Cesium-cesium interactions are explicitly calculated using Kopineck's resonance integral between neighboring wave functions.
4. Conductivity proceeds via cesium-cesium electron tunneling and the conductivity relationship is derived in terms of Kopineck's integral and the surface phonon transitions which supply the conductivity loss mechanism.
5. Phonon energies are explicitly calculated from the vibrational motion of surface atoms.
6. The conductivity varies as the cesium coverage squared, to a first approximation.
7. An equation of state is derived showing the linear dependence of coverage and arrival rate for the low coverage system of interest. The conductivity is then predicted to be proportional to the cesium pressure squared. This prediction has been accurately verified experimentally.

8. By comparing other aspects of theory and experimental data, the heat and entropy change of adsorption have been unambiguously calculated. For all clean alumina and glass substrates $\phi_a = 0.85$ eV and $5.5 < \Delta s/k < 6.2$. The large $\Delta s/k$ values indicate that there is long-range order either caused by dipole-dipole repulsions of surface cesium atoms or by the extended p or d wave functions characteristic of high dielectric materials. A similar long-range order has been observed in LFED studies.
9. For surfaces probably contaminated with hydrogen, conductivity increases above the nonhydrogenated case; the hydrogen probably forms conductivity bridges between nearly cesium atoms. The heat of adsorption is unchanged from $\phi_a = 0.85$ eV, showing that the contaminant affects the conductivity but not the binding energy of cesium.
10. The Arrhenius form of experimental data is convenient for calculating cesium conductivity in various thermionic energy converters and related test apparatus.
11. Sophisticated means have been developed for analyzing the Arrhenius coefficients with and without contaminants. This represents an important tool in understanding the complex system of two adsorbates present on one substrate.

II. WORK FUNCTION STUDIES

by

J. R. Fendley, Jr.

A. CESIUM REFERENCE ANODES*

Cooling of an anode to a temperature slightly above the bulk condensation temperature allows one to attain a readily reproducible anode work function nearly equal to that of bulk cesium. There remains some doubt about the actual value of this work function, but it is substantially higher than the widely quoted value of 1.81 V. A value of $\phi_{cs} = 1.96$ V is presently recommended.

The cesium reference anode technique was applied to measurement of cesium arc drop. Values of arc drop near 0.5 V were found for a rather wide range of cathode temperature, cesium pressure, and spacing variation.

B. A CESIUM BEAM METHOD FOR WORK FUNCTION MEASUREMENT

1. Introduction

Several methods have been used for measuring the work function of metal surfaces coated with an adsorbed layer of cesium. The classic low-current thermionic emission method is exemplified by the work of Taylor and Langmuir.²⁴ In this method, guard rings serve to define the cathode area and minimize the effect of envelope insulator leakage currents. The Marchuk plasma anode technique is another thermionic emission method, which has been employed by Houston.²⁵ With the presence of ions, this method permits use of larger current density to minimize leakage problems. The work of Kitrilakis, Shavit, and Rasor²⁶ employed a retarding potential electron collection method.

All three methods mentioned are steady-state equilibrium methods, in which the envelope insulators are subject to the same cesium flux as is incident upon the sample under investigation. A cesium beam technique has been devised which eliminates insulator leakage problems by shadowing these insulators with cold trap surfaces. The simplest molecular beam techniques²⁷ suffice to form a beam of neutral cesium. If desired, beam techniques would also permit controlled introduction of oxygen or other significant gases onto a sample of interest.

2. Details of the Beam Method

A sample under investigation is the target of a flux of neutral cesium and electrons, which pass through the shutter plane of a beam apparatus. The apparatus is shown schematically in Fig. 15. Prior to opening the shutter, the target is cleaned by heating to a sufficiently high temperature. When the shutter is opened, cesium coverage of the sample increases and the work function changes, resulting in an equal change of terminal potential. The raw data are a plot of terminal

* This paper is published in its entirety in *Proceedings of the Thermionic Conversion Specialist Conference*, Cleveland, Ohio, October, 1964, p. 71, and is summarized here.

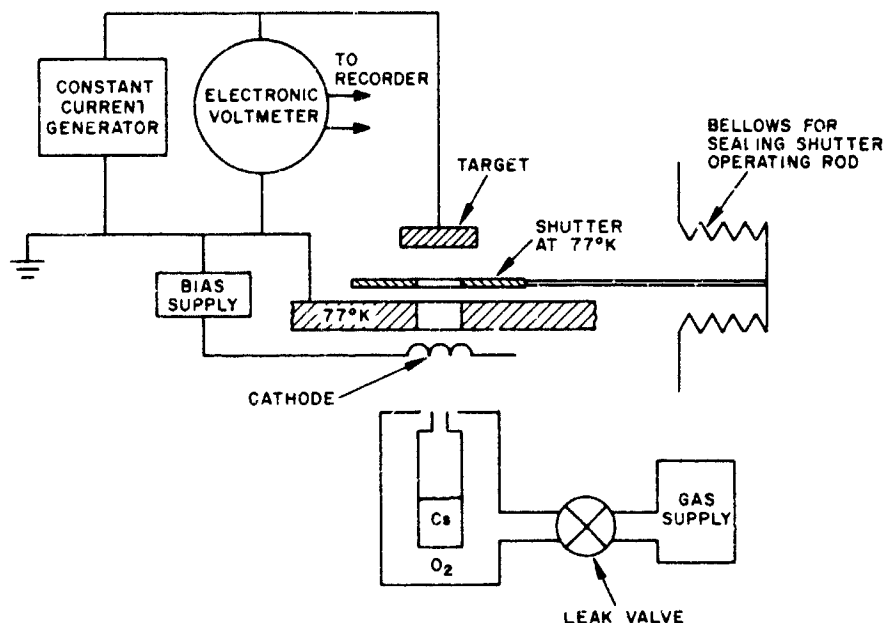


Fig. 15. Beam apparatus for work function measurements.

potential vs. time after shutter opening. The constant current generator and electronic voltmeter are both provided by a single Keithley Model 600 (or similar) electrometer, switched to the OHMS position. Such an instrument has a recorder output proportional to the terminal voltage.

The apparatus is calibrated by use of the cesium reference anode technique.²⁸ This technique eliminates the need for accurate knowledge of cathode temperature, radial current distribution, and space charge effects. When a sufficiently thick film of cesium has collected on the target, the work function is presumed²⁸ to be $1.96 \pm .03$ V.

3. Experimental Results

A preliminary experiment was performed, using apparatus similar to that shown in Fig. 15. Terminal voltage vs. time curves were recorded. Target current of 10^{-8} A and cesium arrival rate of about $10^{12} \text{ cm}^{-2} \text{ sec}^{-1}$ were found to be convenient. Leakage current was less than 10^{-10} A, a negligible value. The cathode used was a hollow cathode similar to that described by Eichenbaum.²⁹ Electrons were accelerated to about 300 V, and then decelerated in the vicinity of the target. Part of the target was shadowed, due to poor alignment of the accelerator electrode with respect to the cathode aperture. This misalignment is thought to be the reason for a failure to observe the expected minima in the terminal voltage vs. time curves. Since a good signal-to-noise ratio was obtained with a target current of only 10^{-8} A, a very simple directly heated tungsten wire cathode should suffice to provide this much current.

Another result of the preliminary experiment was realization of the importance of convenient cycling of the target temperature, preferably without significant change in the target-cathode spacing.

In summary, the transient method described here is recommended for obtaining work function vs. coverage data. There are no leakage problems and other gases such as oxygen may be introduced along with the cesium-electron flux.

III. REVERSE CURRENTS IN THERMIONIC CONVERTERS*

by

K. G. Hernqvist

A general analysis is presented of reverse-current effects which are of importance in cesium arc mode thermionic energy converters.

Two types of reverse-current phenomena are considered, namely: electron flow from the plasma back to the cathode and electron emission from the anode into the plasma. The first phenomenon has two effects: (1) Evaporation cooling of the plasma results in a contribution to the arc drop which may be of the order of 0.1 V. (2) The fully saturated emission current is generally not reached in the power-producing quadrant.

The back emission from the anode has little effect on the net current, but cools the plasma which results in an increased arc drop. As a consequence, an optimum anode work function exists for a specific anode temperature.

The effects of reverse currents on the relationship between arc drop and pressure-distance product are discussed.

* This material has been published in its entirety in the *Proceedings of the Thermionic Conversion Specialist Conference*, Cleveland, Ohio, October, 1964, pages 320-325, and is summarized here.

CONCLUSIONS AND RECOMMENDATIONS

The work described in this report has improved the fundamental understanding of the use of cesium in thermionic converters both for space charge neutralization and for electrode surface conditioning.

New techniques for evaluating the electrode work functions of operating converters have been developed, allowing an accurate determination of the arc drop. The theory of the low-voltage cesium arc has been refined taking into account effects previously neglected. Together, these studies point to the unavoidability of an arc drop of about half a volt. No obvious directions of improvement using a modified geometry or introduction of gas additives have been established.

In the area of electrode surface properties theoretical device limits have not yet been achieved. The achievement of lower work functions will lead to device improvement, particularly in the area of collector properties. Further advances, however, necessitate adding another constituent to the cesium on metal system presently used. The work on adsorption of cesium on insulators described in this report has provided fundamental knowledge of value for an understanding of the more complicated system using two adsorbates for electrode surface conditioning. It is recommended that further theoretical and experimental studies be made on such a system. The theoretical approaches described in this report should be extended to metals with the aid of Wannier functions. Experimental studies using beam techniques should be applied to the two-adsorbate system.

In summary, the following conclusions and recommendations are made based on the work described in this report:

1. An arc drop of about $\frac{1}{2}$ volt seems unavoidable for the present form of thermionic converters. No obvious ways to improving this requirement without decreasing device reliability have been established.
2. Lowering of electrode surface work functions is possible and will lead to device improvement. Further studies of the two-adsorbate system are recommended.

REFERENCES

1. J. D. Levine, *Proceedings of the Thermionic Conversion Specialist Conference*, Cleveland, Ohio, October, 1964, p. 1.
2. J. D. Levine, Vapor-Filled Thermionic Converters, Mid-Point Report, (NASA CR-54194), September, 1964.
3. B. L. Blackford, Electronic Research Laboratory, MIT, Quarterly Progress Report **68**, 2 (1963).
4. J. Koutecky, *Trans. Faraday Soc.* **51**, 1038 (1958); *J. Surface Science* **1**, 280 (1964).
5. T. B. Grimley, *J. Phys. Chem. Solids* **14**, 227 (1960).
6. T. A. Hoffman, *Hungarica Acta Physics* **2**, 195 (1952).
7. P. B. Weisz, *J. Chem. Phys.* **21**, 1531 (1953).
8. K. Hauffe, *Semiconductor Surface Physics*, edited by R. H. Kingston, (University of Pennsylvania Press, Philadelphia, Pa., 1956).
9. N. F. Mott and R. W. Gurney, *Electronic Processes in Ionic Crystals*, (Dover Publications, New York, 1964), p. 82.
10. W. Kohn, *Solid State Physics* **5**, 257 (1957).
11. R. H. Bube, *Solid State Physics* **11**, 223 (1960).
12. L. Pauling and E. B. Wilson, *Introduction to Quantum Mechanics*, (McGraw-Hill Book Co., Inc., New York, 1935), p. 132.
13. L. I. Schiff, *Quantum Mechanics*, (McGraw-Hill Book Co., Inc., New York (1955), p. 30.
14. E. Arnold and A. Patterson Jr., "Calculation of Conductivity in Sodium-Liquid Ammonia Solutions," in *Metal-Ammonia Solutions*, edited by G. Lepoutre and M. J. Sienko, (W. A. Benjamin, Inc., New York 1964), p. 160.
15. L. Pauling, *Introduction to Quantum Mechanics*, (McGraw-Hill Book Co., Inc., New York, 1935).
16. H. Kopineck, *Z. Naturforsch.* **5a**, 420 (1950).
17. K. B. Wiberg, *Physical Organic Chemistry*, (John Wiley and Sons, Inc., New York, 1964), p. 469.
18. J. H. deBoer, "Adsorption Phenomena" in *Advances in Catalysis VIII*, (Academic Press, New York, 1956), p. 120.
19. J. Topping, *Proc. Roy. Soc. (London)* **A114**, 67 (1927).
20. I. Langmuir, *J. Am. Chem. Soc.* **54**, 2798 (1932).
21. J. B. Taylor and I. Langmuir, *Phys. Rev.* **44**, 423 (1933).
22. J. D. Levine and E. P. Gyftopoulos, "Adsorption Physics of Metals Partially Covered by Metallic Particles. II. Desorption Rates of Atoms and Ions," *J. Surface Science* **1**, 225 (1964).
23. J. D. Levine and E. P. Gyftopoulos, "I. Atom and Ion Desorption Energies," *J. Surface Science* **1**, 171 (1964).
24. J. B. Taylor and I. Langmuir, *Phys. Rev.* **44**, 454 (1933).
25. J. M. Houston, *Advances in Electronics* **17**, 125 (1962). See also *Proceedings of the Thermionic Conversion Specialist Conference*, Cleveland, Ohio, October, 1964, p. 77.

REFERENCES (Cont'd)

26. S. S. Kitrilakis, A. Shavit and N. R. Rasor. Report on 24th Annual Conference on Physical Electronics, MIT, Cambridge, Mass. p. 171. 1964.
27. N. F. Ramsey, *Molecular Beams*, (Oxford Clarendon Press, 1956).
28. J. R. Fendley, Jr., *Proceedings of the Thermionic Conversion Specialist Conference*, Cleveland, Ohio, October, 1964, p. 71.
29. A. L. Eichenbaum, *RCA Rev.* **23**, 230 (1962).